JOINT INSTITUTE FOR AERONAUTICS AND ACOUSTICS

JIAA TR 115

Stanford University

APPLICATION OF THE PRESSURE SENSITIVE PAINT TECHNIQUE TO STEADY AND UNSTEADY FLOW

Y. Shimbo, R. Mehta, B. Cantwell

Department of Aeronautics and Astronautics
Stanford University
Stanford, CA 94305

June 1996

ABSTRACT

Pressure sensitive paint is a newly-developed optical measurement technique with which one can get a continuous pressure distribution in much shorter time and lower cost than a conventional pressure tap measurement. However, most of the current pressure sensitive paint applications are restricted to steady pressure measurement at high speeds because of the small signal-to-noise ratio at low speed and a slow response to pressure changes. In the present study, three phases of work have been completed to extend the application of the pressure sensitive paint technique to low-speed testing and to investigate the applicability of the paint technique to unsteady flow.

First the measurement system using a commercially available PtOEP/GP-197 pressure sensitive paint was established and applied to impinging jet measurements. An in-situ calibration using only five pressure tap data points was applied and the results showed good repeatability and good agreement with conventional pressure tap measurements on the whole painted area. The overall measurement accuracy in these experiments was found to be within 0.1 psi.

The pressure sensitive paint technique was then applied to low-speed wind tunnel tests using a 60 deg delta wing model with leading edge blowing slots. The technical problems encountered in low-speed testing were resolved by using a high grade CCD camera and applying corrections to improve the measurement accuracy. Even at 35 m/s, the paint data not only agreed well with conventional pressure tap measurements but also clearly showed the suction region generated by the leading edge vortices. The vortex breakdown was also detected at α=30 deg. It was found that a pressure difference of 0.2 psi was required for a quantitative pressure measurement in this experiment and that temperature control or a parallel temperature measurement is necessary if thermal uniformity does not hold on the model.

Finally, the pressure sensitive paint was applied to a periodically changing pressure field with a 12.8s time period. A simple first-order pole model was applied to deal with the phase lag of the paint. The unsteady pressure estimated from the time-changing pressure sensitive paint data agreed well with the pressure transducer data in regions of higher pressure and showed the possibility of extending the technique to unsteady pressure measurements. However, the model still needs further refinement based on the physics of the oxygen diffusion into the paint layer and the oxygen quenching on the paint luminescence.

ACKNOWLEDGMENT

TABLE OF CONTENTS

LIST OF TABLES

LIST OF FIGURES

LIST OF FIGURES (Continued)

NOMENCLATURE

A,B	Constants for pressure sensitive paint calibration
A_j	Area of the blowing slot
$C\mu$	Momentum coefficient of the jet
Cp	Pressure coefficient
D	Jet nozzle diameter
Dm	Diffusion constant
Error	Total error for the pressure estimation
I	Local pressure sensitive paint luminescence
I_0	Pressure sensitive paint luminescence at vacuum
Ir	Pressure sensitive paint luminescence at reference pressure
K	Gain of the first-order pole
Nmax	Full well depth of the CCD camera
P	Local pressure
Patm	Atmospheric pressure
Peff	Effective pressure at time t
Pest	Estimated pressure at time t
Pmax	Maximum pressure on the flat plate
PO_2	Partial pressure of oxygen
Pref	Reference pressure
S	Reference area of the model
T	Temperature
T'	Temperature at on-wind condition
T_0	Temperature at reference condition
U	Free-stream velocity in the test section
V_j	Jet velocity from the blowing slot
X	Coordinate perpendicular to the paint surface (X=0 at paint surface)
a(T)	Stern-Volmer coefficient
b	Span of the model
c	Center-line chord length of the model
d	Paint layer thickness
dCp	Difference in Cp
dP	Difference in pressure

Nomenclature (Continued)

f	Frequency of the pressure oscillation
h	Planck's constant or proportional constant for Henry's law
k	Boltzman's constant
k_A	Chemical reaction velocity of excitation
k_C	Chemical reaction velocity of internal conversion
k_F	Chemical reaction velocity of emission
k_q	Chemical reaction velocity of oxygen quenching
s	Local coordinate along the upper surface of the model
smax	s at the leading edge
t	Time or slot opening of the model
x	Axis of the flat plate in horizontal direction (x=0 at P=Pmax) or Distance along the center line of the model (x=0 at apex)
y	Axis of the flat plate in vertical direction (y=0 at P=Pmax)
$\Delta Ptap$	Error in pressure transducer measurement
Φ	Quantum efficiency
Φ_0	Quantum efficiency at vacuum
α	Angle of attack
β	Sideslip angle
εp	Pressure error due to the shot noise of the CCD camera
η	Mole fraction of the oxygen in air (=0.21)
ν	Frequency of the excitation light
ν'	Frequency of the emission light
θ	Jet impinging angle
ρ	Density of the air
τ	Time constant of the first-order pole
$[O_2]$	Concentration of the oxygen molecules

Nomenclature (Continued)

(A or B)' Constants for pressure sensitive paint calibration with temperature difference between measurement and reference conditions

$( )_1$ Value at lower pressure region

$( )_2$ Value at higher pressure region

$( )_c$ Value at an intersecting point

$( )_j$ Value for j th group

$( )_k$ Value at k th data point

Chapter 1 Introduction

This thesis summarizes the development of a pressure sensitive paint measurement system and its application to low-speed testing and unsteady pressure measurements.

Surface pressure measurements are one of the most important measurements both, for airplane development and for aerodynamics research. Pressure distribution data give us an insight into the flow field, and they are useful for evaluating the aerodynamic design of an airfoil or a wing planform. In addition, these data are essential for the structural and equipment design of the aircraft. For example, detailed pressure distributions enable one to determine dimensions of the structures and the locations of the air inlets.

In airplane development, more than 300 points of pressure all over the airplane surface are usually measured in a wind tunnel using a scaled model after the preliminary configuration is fixed. The most popular and conventional way to measure surface pressures is a combination of a pressure tap and a pressure transducer, as shown in Figure 1.1. The pressure tap is a tiny hole drilled perpendicular to the surface and it is connected through a vinyl tube to the pressure transducer, which converts the pressure into an electrical signal. In case the pressures at many points are measured at the same time, a mechanical pressure scanning system such as the one made by Scanivalve has been widely used so that up to 45

points of pressure can be measured by only one pressure transducer. Recently electric pressure scanning systems such as the PSI system and the ZOC valve are becoming popular because these electric systems are much faster than the mechanical scanning systems. However, there are two disadvantages in the conventional method. First, the conventional method is a point measurement, in which one can measure the pressure only at a restricted number of points where the pressure taps are located. Consequently, one has no idea about the spatial variation of the pressure in regions where no pressure taps are installed. Therefore, one has to make a very careful decision where to put the pressure taps, depending on what kind of pressure data one is interested in. Second, the conventional method is costly and time consuming, both in the wind tunnel model development and test preparation processes. Drilling tiny holes perpendicular to a curved model surface and connecting them to vinyl tubes is sometimes very difficult, especially for very thin and small models. In addition, one has to spend a good deal of time connecting a large number of pressure tubes and checking for leakage through the tubes.
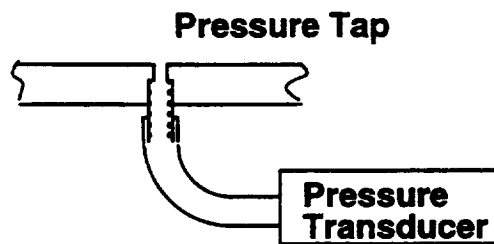
Figure 1.1 Conventional pressure measurement technique

Pressure sensitive paint, on the other hand, is a newly-developed pressure measurement technique in which the surface pressure distribution on an aerodynamic body is measured optically, with a special kind of paint applied on the surface. Figure 1.2 shows a schematic of the technique. The painted surface is illuminated by a light source of a particular wavelength and the luminescence of the paint is measured as a light intensity field. One of the greatest features of the pressure sensitive paint technique is that it is a continuous pressure field measurement. One can get much more information about a flow field because pressure information is available anywhere the pressure paint is applied as long as optical access to the relevant areas is available. One does not have to spend time deciding where to put the restricted number of pressure taps, and the paint data are also useful for the validation of computational fluid dynamics(CFD) codes. Another advantage of this technique is the much lower cost and shorter time involved in wind tunnel testing and model development for pressure measurements. With the pressure sensitive paint applied

2

to the surface, the wind tunnel test model no longer needs a large number of pressure taps and therefore, the pressure measurement can be conducted much more easily and less expensively in a shorter period. This advantage finally leads to a faster and less expensive development of the aircraft itself.
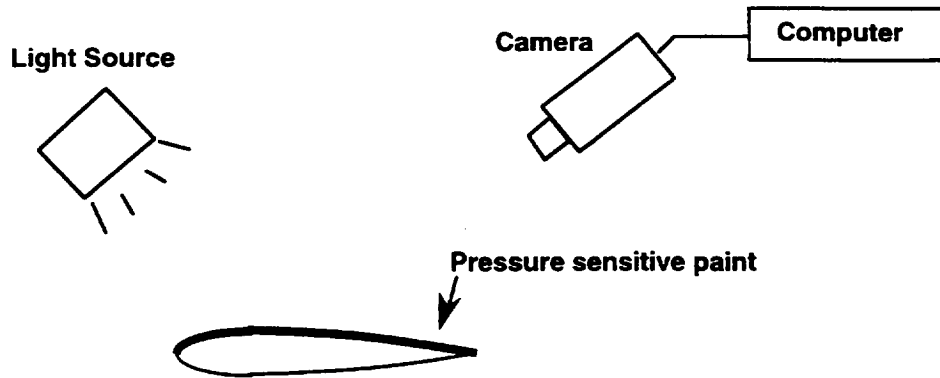
Figure 1.2 Pressure sensitive paint technique

The pressure sensitive paint technique, therefore, is becoming more popular, both in academic and industrial fields. Several research institutes have developed their own paints and measurement techniques (Ref. 1-9). However, at present, most of the pressure sensitive paints are not commercially available and these applications are mostly restricted to steady pressure measurements at high speeds. The reason for this restricted application is that the measurement accuracy tends to become poor at low speeds where the pressure difference generated by the air flow is usually very small leading to relatively small signal-to-noise ratios. Another problem is that the response of the pressure sensitive paint to pressure changes is too slow to be applied to unsteady pressure measurements.

With this background, the objectives of this research are first, to establish the basic pressure sensitive paint measurement technique with a commercially available paint, second, to expand its application to low-speeds and third, to investigate the applicability of the paint technique to unsteady pressure measurements. These expansions will make the pressure sensitive paint a much more useful and more popular experimental technique and it will be applied in solving the aerodynamic problems such as unsteady and complex flow fields around fighter-type airplanes and helicopter rotor blades.

3

In this thesis, the basic measurement principles are described in Chapter 2 and the details of the three steps of work: impinging jet measurements, low-speed wind tunnel tests and unsteady pressure measurements are described in Chapters 3,4 and 5, respectively. Finally, Chapter 6 concludes the research and discusses some future work.

Chapter 2   Measurement Principles

2.1 Basic Principles

The pressure sensitive paint is composed of a luminescent substance (luminophor) and an oxygen permeable binder. Figure 2.1.1 shows the structure of a typical pressure sensitive paint layer and Figure 2.1.2 illustrates the typical optophysical characteristics of the luminophor. The basic principle of the pressure sensitive paint technique is a diffusion of the oxygen molecules into the paint layer and the oxygen quenching of excess energy released by the luminophor when excited by a light of the proper wavelength.

The luminophor is excited from its initial singlet ground energy state, S_0, to a higher singlet energy state, Si (i > 1), by absorbing a photon energy from the illuminating light of particular wavelength. However, any higher excited energy state Si (i > 2) is rapidly relaxed into the lowest excited state S_1 through an internal conversion process. Then it drops to the ground state S_0 again either by emitting a photon with longer wavelength than it absorbed or through radiationless deactivation processes. Oxygen quenching is one of the radiationless deactivation processes in which the luminophor in its excited state loses its energy through a collision with an oxygen molecule and returns to the ground state without

5

emitting light. Another radiationless deactivation process is internal conversion which converts the excess energy into heat.
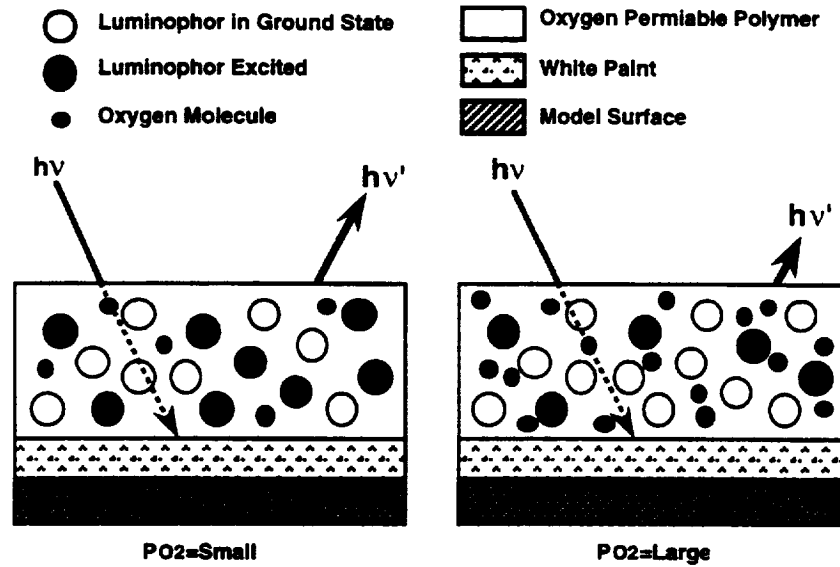
Figure 2.1.1 Typical pressure sensitive paint layer
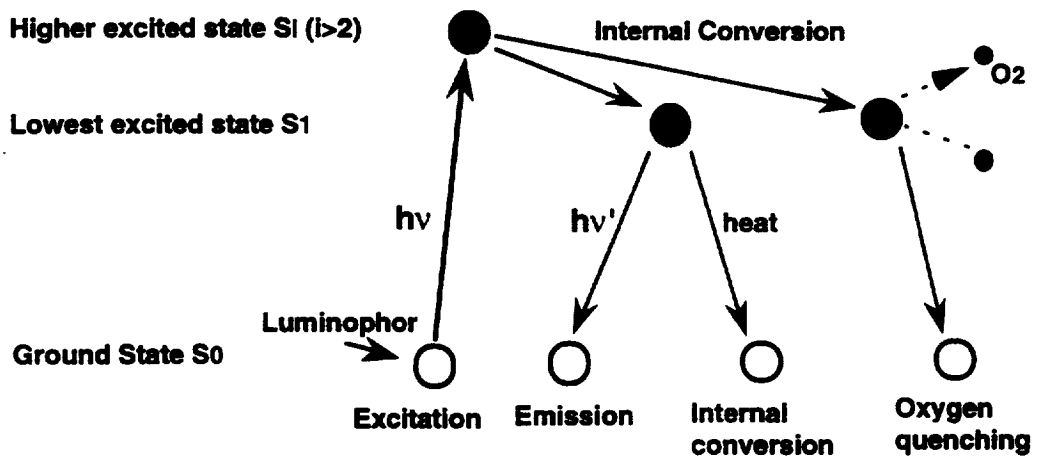
Figure 2.1.2 Photophysical characteristics of the luminophor

6

When the pressure sensitive paint is applied on a model surface, both the luminophor and the oxygen permeable binder are dissolved into a certain solvent and then brushed or sprayed over the white paint layer put on the surface as an undercoat. The solvent evaporates after the paint has dried and the oxygen permeable paint layer with the luminophor distributed in it is formed on the surface. The two roles of the white paint applied between the model surface and the pressure sensitive paint layer are to reflect the illuminating light so that it is well absorbed by the luminophor distributed in the paint layer, and to bind the paint layer firmly to the model surface.

2.2 Governing Formulae

In an equilibrium condition, the diffusion process of the oxygen molecules into the paint layer is subject to Henry's law:

$$[O_2] = hP_{O_2} \qquad (2.2.1)$$

In our surrounding air, the mole fraction of the oxygen is known to be $\eta=0.21$ and the partial pressure of oxygen can be easily replaced by the pressure of air as:

$$[O_2] = h\,(\eta P) \qquad (2.2.2)$$

Ref. 6 describes the photophysical process of the luminescent substance M as:

Process	Reaction	Rate
Excitation	$h\nu + M \rightarrow M^*$	k_A
Emission	$M^* \rightarrow M + h\nu`$	k_F
Internal conversion	$M^* \rightarrow M + heat$	k_C
Oxygen quenching	$M^* + O_2 \rightarrow M + O_2$	$k_q\,[O_2]$

where * indicates the excited energy state. To quantify the luminescence from the paint, the quantum efficiency Φ is introduced as:

$$\Phi = \frac{photon\ \ emitted}{photon\ \ absorbed} \qquad (2.2.3)$$

and it is rewritten using the chemical reactions above as:

$$\Phi = \frac{k_F}{k_A} \qquad (2.2.4)$$

In the equilibrium condition, the relation:

$$k_A = k_F + k_C + k_q \, [O_2] \qquad (2.2.5)$$

holds and therefore the quantum efficiency is descried as:

$$\Phi = \frac{k_F}{k_F + k_C + k_q[O_2]} \qquad (2.2.6)$$

If there is no oxygen, the quantum efficiency becomes:

$$\Phi_0 = \frac{k_F}{k_F + k_C} \qquad (2.2.7)$$

and the luminescence from the paint is at its maximum value, I_0.

Under the same excitation condition at temperature T, the Stern-Volmer relation is introduced as:

$$\frac{I_0}{I} = \frac{\Phi_0}{\Phi} = 1 + a(T)P \qquad (2.2.8)$$

where the Stern-Volmer coefficient,

$$a(T) = \frac{\eta h k_q}{k_F + k_C} \qquad (2.2.9)$$

is a function of temperature because both the oxygen diffusion and the chemical reaction (oxygen quenching) are highly dependent on the temperature.

In a real operation at temperature $T=T_0$, it is hard to measure I_0, the luminescence from the paint under a vacuum condition, and instead, luminescence, Ir, at a given reference pressure, Pref, is measured, which yields:

$$\frac{I_0(T_0)}{I_r(Pref, T_0)} = 1 + a(T_0)Pref \qquad (2.2.10)$$

In the same manner, the luminescence, I, at an unknown pressure, P, yields:

$$\frac{I_0(T_0)}{I(P, T_0)} = 1 + a(T_0)P \qquad (2.2.11)$$

8

By dividing Eq. (2.2.11) by Eq. (2.2.10), the nondimensional relationship is introduced as:

$$\frac{Ir(Pref, To)}{I(P, TO)} = \frac{Io(To)/I(P, To)}{Io(To)/Ir(Pref, To)} = \frac{1 + a(To)P}{1 + a(To)Pref}$$

$$= A(To) + B(To)\left(\frac{P}{Pref}\right) \qquad (2.2.12)$$

$$A(To) = \frac{1}{1 + a(To)Pref} \qquad (2.2.13)$$

$$B(To) = \frac{a(To)Pref}{1 + a(To)Pref} \qquad (2.2.14)$$

and it should be noted that,

$$A(T_0) + B(T_0) = 1 \qquad (2.2.15)$$

Eq. (2.2.12) indicates that once the reference condition is fixed, the relation between the luminescence ratio (Ir/I) and the pressure ratio (P/Pref) is expressed by a straight line going through the point (1,1). Therefore, once the two constants $A(T_0)$ and $B(T_0)$ in Eq. (2.2.12) are determined through a calibration and reference data are measured, the unknown pressure (P) can be computed by measuring the luminescence (I) from the paint. This non-dimensionalization process also eliminates the effect of nonuniform paint thickness and nonuniform illumination from the light source.

One of the problems of the pressure sensitive paint technique is the rather strong temperature dependency. As is described above, the Stern-Volmer constant a(T) is a function of temperature and the formulae of A and B derived in Eq. (2.2.13) and (2.2.14) are valid only if the temperature is constant between the measurement and reference conditions. Therefore, any temperature nonuniformity on the surface becomes an error source unless the temperature distribution is measured simultaneously.

Another problem of the pressure sensitive paint technique is a degradation of the paint. When the paint layer is illuminated by a light source for a long time, its characteristics change and luminescence from the paint decreases even under the same pressure and temperature conditions. If the degradation occurs between the measurement and reference conditions, the calibration constants A and B change and this leads to an error. Therefore the illumination of the paint should be long enough for a stable photon absorption but at the same time it should be kept as short as possible.

9

2.3 Paint Calibration

There are two kinds of paint calibration methods widely used, namely, an in-situ calibration and an a priori calibration.

In the in-situ calibration, only the pressure tap data obtained simultaneously or under the same conditions as the paint image acquisition are used for the calibration. In this calibration, the pressure tap data are related to the luminescence ratio of the paint corresponding to their locations. The advantage of the in-situ calibration is that one does not have to worry about the temperature difference and the paint degradation between the measurement and reference conditions because these effects are automatically included in the calibration constants A and B. But, one still needs some pressure taps installed on the surface.

In the a priori calibration, on the other hand, calibration is conducted using a pressure chamber where both the pressure and temperature are arbitrary controlled. Once a complete set of luminescence ratio data at all combinations of temperature and pressure are obtained, one can handle the temperature change between the measurement and reference conditions. However, one has to measure the surface temperature accurately and this is difficult if there is spatial variation of temperature on the model. In addition, there is no way to deal with paint degradation between these two conditions.

Chapter 3   Impinging Jet Measurements

A shop-air jet impinging on a flat plate was chosen as an experimental set-up because it was a very easy way to generate a desired pressure change and there was no conflict with the heavily used wind tunnels. A basic pressure sensitive paint measurement system was established and the measurement accuracy was evaluated through the impinging jet measurements.

3.1 Experimental Set-up

(1) Experimental set-up

The experimental set-up for the impinging jet measurements is shown in Figure 3.1.1.

(A) Jet nozzle

A brass air hose connector was used as a jet nozzle. The nozzle was connected to the high pressure supply through a 50 psi line via a regulator. The air hose diameter was at least 1/4 inch to avoid choking at the minimum area location.

11
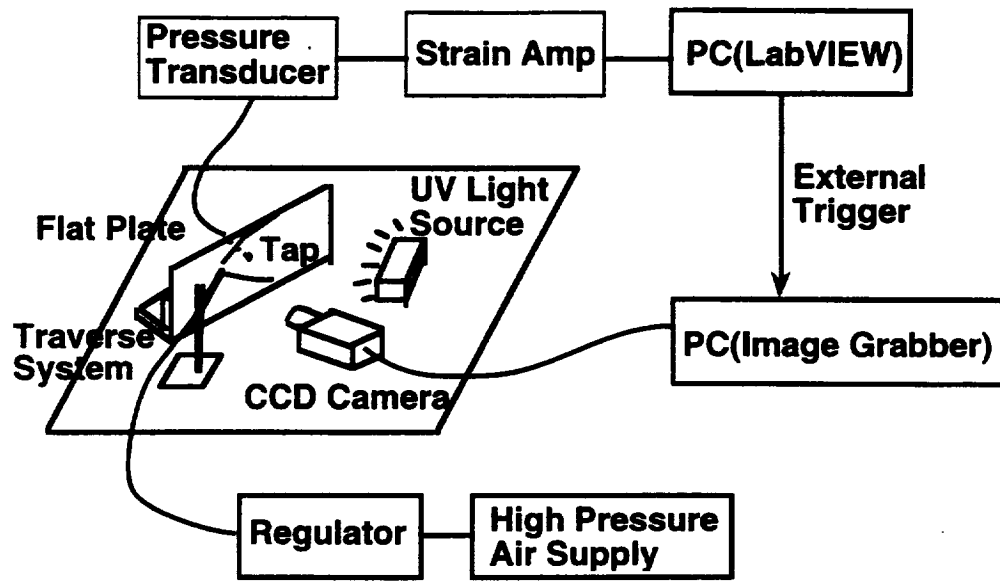
(a) Schematic
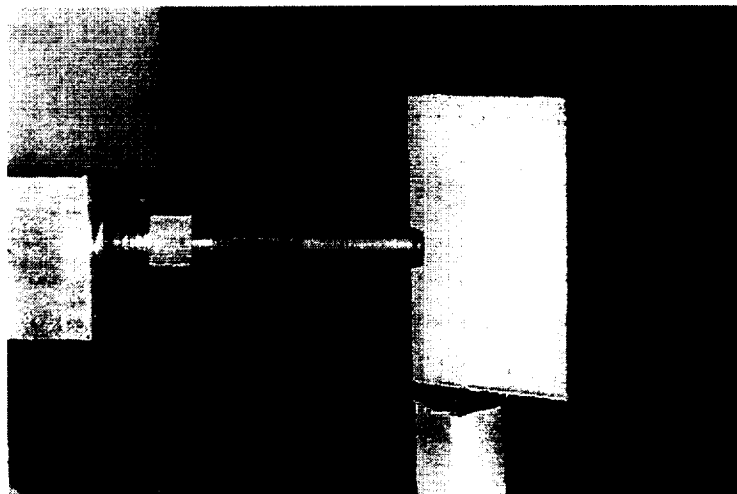
(b) Painted region

Figure 3.1.1 Experimental set-up for the impinging jet measurements

(B) Traverse system

The jet nozzle was mounted on a traverse system. The jet nozzle location and the jet impinging angle were adjusted by the traverse system and the setting was repeatable.

(C) Flat plate

The flat plate was an 8"x11" aluminum plate with 1/8" thickness. The pressure sensitive paint was applied on a 2" x 2" square region of the surface and the plate was also equipped with 121 pressure taps for conventional pressure measurements. These taps are located at the grid points of 11 rows and 11 columns aligned at every 1/4". Each pressure tap has a 1/64" diameter on the surface and it was connected to the stainless tube with a 1/32" inch inner diameter and a 1/16" outer diameter. Then, each stainless tube was connected to the pressure transducer through a long vinyl tube with a 1/16" inner diameter.

(D) Pressure sensitive paint

The pressure sensitive paint used in this research was provided by NASA Ames Research center. It was a very basic combination of Platinum Octaethyle Porphyrin (PtOEP) and GP-197. PtOEP is a luminophor originally developed by the University of Washington and it is now commercially available from Porphyrin Products in Utah (Tel 801-753-1901). The excitation wavelength is 365 nm in the UV region and the emission wavelength is 650 nm in red. The chemical formula and the spectral characteristics of PtOEP from Ref. 4 are shown in Figure 3.1.2. GP-197 is a resin solution and it is also commercially available from Genessee Corporation in Michigan (Tel 313-238-4966). The mixture ratio of these two substances was 9.4 mg of PtOEP dissolved in 100 ml of GP-197, as described in Ref. 4. In the painting process, a glossy white paint (Krylon 91501) was applied first on the surface as an undercoat and then the pressure sensitive painted was air-brushed over the white paint.

(E) Light source

The light source used was a UV light with 365 nm wavelength (Electro-Lite Corporation, ELC-250 Blacklight lamp and ELC-2540 Power Supply). This light was also borrowed from NASA Ames Research Center.
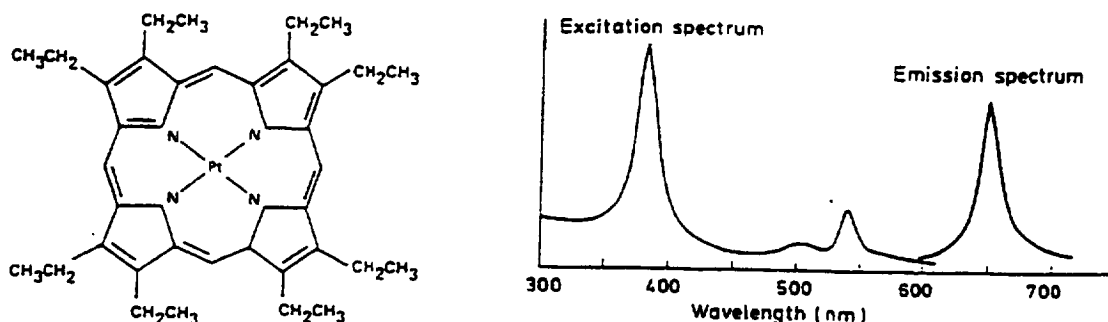
Figure 3.1.2 Chemical formula and spectrum characteristics of PtOEP (Ref. 4)

(F) CCD camera

The paint image was recorded by a PULNiX TM-745 CCD camera with a CCU-84 camera controller. The image size of this camera was 512 x 512 pixels and a 50 mm Nikon standard camera lens was used. A 650 nm wavelength bandbass filter (Melles Griot 03FIV022) was attached to the lens so that only the emission from the pressure sensitive paint was captured. The aperture was set to f=1.8 to make the paint image as bright as possible and the exposure time of each frame was 50 ms in which every other horizontal pixel row was scanned simultaneously.

(G) Image grabber

The image grabbing board/software used in this experiment was Pixel tool 5.0 distributed by Perceptics Corporation. It is a monochrome image grabber with an 8 bit light intensity resolution. This system can store up to 16 images in 512x512 pixel array in its own memory and therefore it is capable of capturing sequential images up to 8.5 seconds interval. This system also has an option to start taking sequential images by an external trigger signal (positive slope from TTL low to TTL high voltage).

(H) Pressure transducers

Five pressure transducers were used in this experiment. Two of them were the same pressure transducers with 2.5 psi capacity and the other three transducers were 2 psi capacity. In the impinging jet measurements, all of these five pressure transducers were used, connected to the pressure taps through long vinyl tubes.

14

(I) Data acquisition system

A 12 bit A/D conversion board (National Instruments) was used for the data acquisition of the pressure transducers. An in-house LabVIEW program on the Macintosh II personal computer was used to control the test sequence and to measure the pressure transducer data.

(2) Test sequence

Test cases of the impinging jet measurements are shown in Table 3.1.1 and the notation for this experiment is shown in Figure 3.1.3.

(A) Test sequence

Seven sets of experiments were conducted for each jet blowing condition. First, for a given jet blowing condition, pressure sensitive paint images and pressure tap data at five points for an in-situ calibration were obtained simultaneously. Next, the pressure tap measurement with 30 taps were conducted for the same blowing condition. Then, three sets of pressure tap measurements were conducted at 30 pressure tap locations for the same jet blowing condition, but the nozzle location was shifted $(x,y)=(1/8",0)$, $(1/8", 1/8")$ and $(0, 1/8")$, respectively. As the pressure taps were aligned in $1/4"$ interval, these three pressure tap measurements effectively increased the spatial resolution of the pressure tap measurement up to 120 points within the painted area. Finally, the nozzle was returned to the original location and the pressure sensitive paint with five pressure taps measurements were conducted again, followed by another pressure tap measurement at 30 points. A test case to represent the jet blowing condition was chosen from two pressure sensitive paint results and it is indicated by the italic bold-face in Table 3.1.1.

For the pressure measurements at 30 pressure tap locations, the jet was blown eight times under the same conditions. One of the five pressure transducers was fixed to a specific pressure tap location for monitoring the jet blowing condition and the other four transducers were switched among pressure taps each time.

15

Table 3.1.1 Test cases — Impinging jet measurements

Jet blowing condition				Case							
D	r/D	Theta	Pmax	PSP	X					X	
(inch)		(deg)	(psi)	# Tap	5	30	30	30	30	5	30
				x@Pmax	0	0	1/8"	1/8"	0	0	0
				y@Pmax	0	0	0	1/8"	1/8"	0	0
0.298	4	45	1.4		31	32	33	34	35	*36*	37
0.298	2	45	1.8		*38*	39	40	41	42	43	44
0.298	2	45	1.4		45	46	47	48	49	*50*	51
0.298	2	45	1		*52*	53	54	55	56	57	58
0.298	1.08	45	1.4		59	60	61	62	63	*64*	65
0.155	2	45	1.8		*66*	67	68	69	70	73	74
0.298	2	22.5	1.4		81	82	83	84	85	*86*	87
0.298	2	45	1.4		88	89	90	91	92	*#93*	94
0.298	1.08	45	1.4		*#95*	96	97	98	99	100	101
0.298	2	67.5	1.4		*#102*	103	104	105	106	#107	108
0.298	2	90	1.4		*109*	110	111	112	113	114	115

Bold number indicates the case used for a parametric study
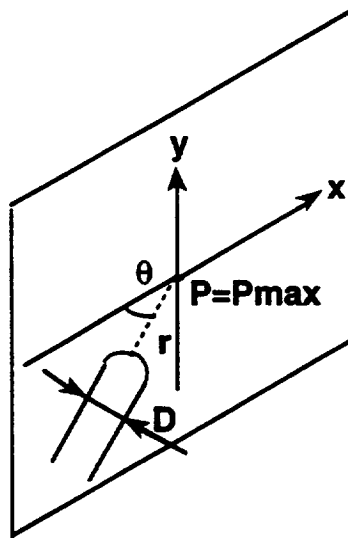
# indicates the 30 points calibration

Figure 3.1.3 Parameters and notations used in the impinging jet measurements

(B) Image acquisition

The sequence of the image data acquisition is shown in Figure 3.1.4. Each pressure sensitive paint image was recorded on a 320 x 320 pixel array. First, 16 dark current images were acquired with a cap on the lens of the CCD camera to account for the camera dark current noise. This sequence was done only once a day and the dark current images were commonly used for the other cases of the day. In each case, 16 initial images were taken in advance to the jet blowing and then, jet is turned on and 16 on-wind images were taken at the same time as the pressure tap measurements. Finally, after the jet is turned off, 16 final images were taken. All these 16 images were taken sequentially in 1/30 second interval. The time required from initial image acquisition to final image acquisition was about 15 minutes, including the saving process of the images.
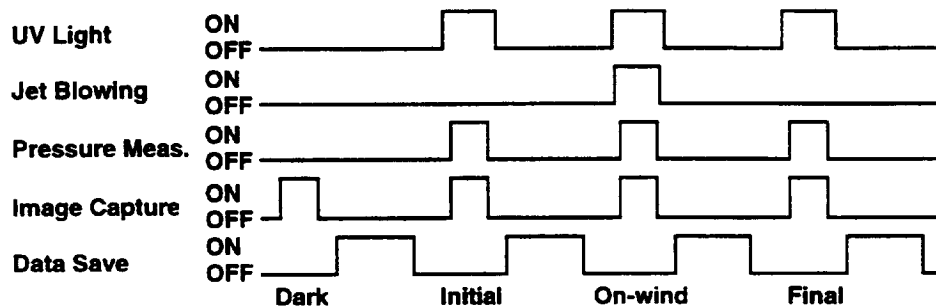
Figure 3.1.4 Sequence of the image data acquisition

(C) Pressure data acquisition

Pressure transducer data were acquired simultaneously with the image acquisition. The LabVIEW program controlling the test sequence, sent a trigger pulse to the image grabber for starting the image acquisition and also generated another pulse at the moment the last image was taken. For the on-wind condition, pressure transducer data were sampled at 50 Hz sampling rate from several hundred milliseconds prior to the first image acquisition to several hundred milliseconds after the last image acquisition, and then, the pressure transducer data acquired during the image acquisition were averaged. On the initial and final no-wind conditions, pressure transducer data were also sampled at 50 Hz and 100 data points were averaged. The pressure measurements without image acquisition were also conducted in the same way as the no-wind measurements.

17

3.2 Data Reduction

The sequence of the data reduction is shown in Figure 3.2.1.

$$\frac{Ir}{I} = \frac{(No\text{-}Wind)\text{-}Dark}{(On\text{-}Wind)\text{-}Dark}$$
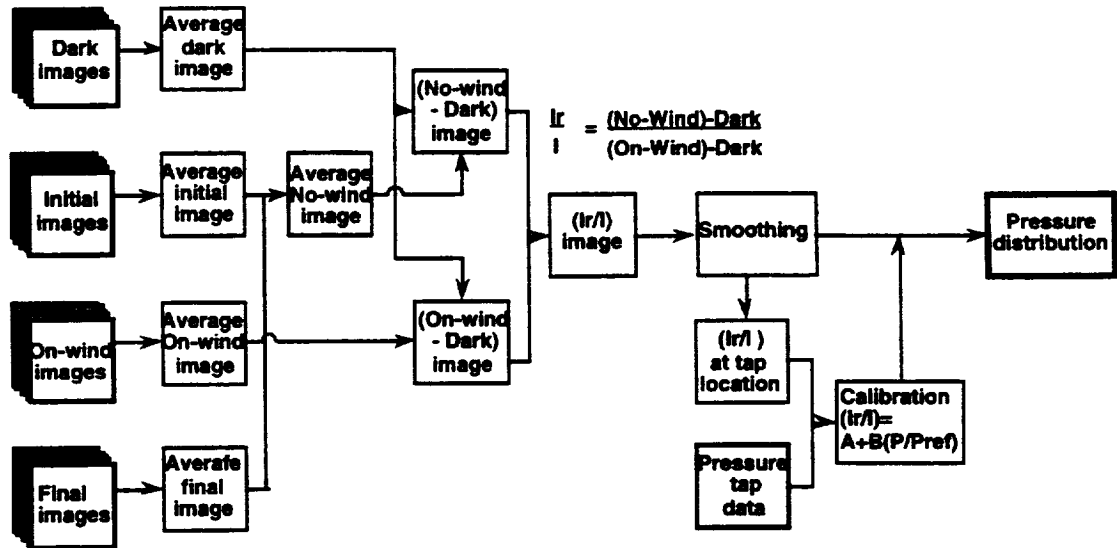
Figure 3.2.1 Flowchart of the data reduction

(1) Averaging

First, 16 images in each of dark, initial, on-wind and final condition were summed up, which was equivalent to a time average at the same condition. This procedure helped to reduce the noise, such as camera shot noise and electro-magnetic interference with some other instruments and consequently, improved the signal-to-noise ratio of the image. The effect of averaging in this particular experiment is shown in Figure 3.2.2. For a total of 19 no-wind measurements, the average luminescence at one fixed point using different number of images is compared with the average of 16 images. As the number of images averaged is increased, the scatter from the average of 16 images reduces significantly. In this experiment, the average was limited to 16 images because the image grabber can store only sixteen 320 x 320 pixel images in its memory.
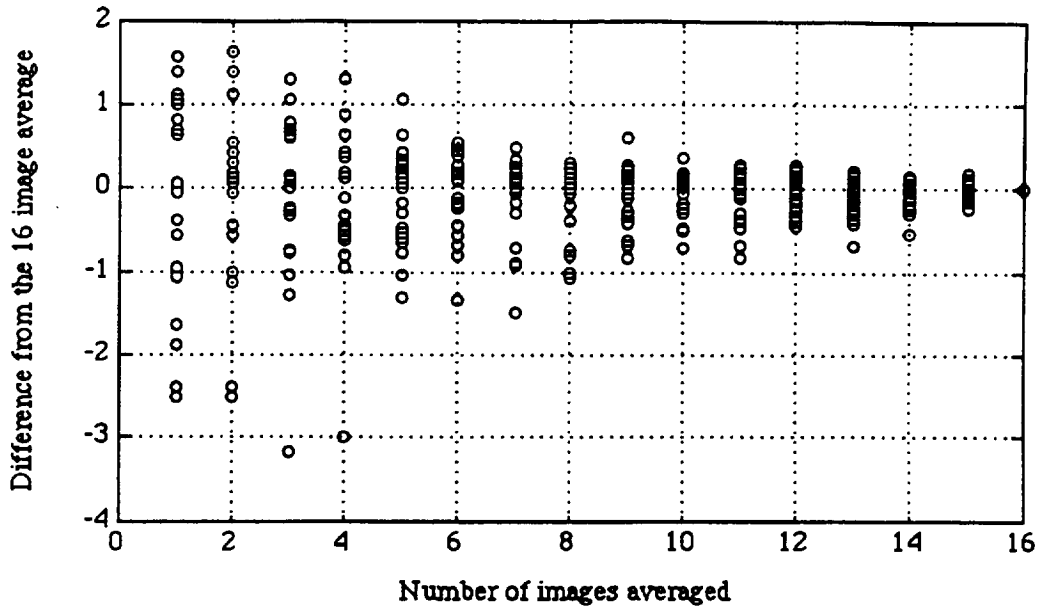
Figure 3.2.2 Averaging effects

(2) Luminescence ratio image

The raw luminescence ratio image was generated by dividing the corrected no-wind image by the corrected on-wind image pixel by pixel. Here, the corrected on-wind image was generated by subtracting the summed-up dark image from the summed-up on-wind images and this process took care of the initial drift or offset of each pixel of the CCD camera. The corrected no-wind image was generated by averaging the summed-up initial and final images and then subtracting the summed-up dark image. Then, a final luminescence ratio image was created by applying a two-dimensional smoothing to the raw luminescence ratio image. This smoothing process reduced the high spatial frequency component of the image and also enabled the estimation of the luminescence ratio at the pressure tap locations where no pressure sensitive paint was applied. The effect of smoothing is shown in Figure 3.2.3, both as a whole luminescence ratio image and line plots across the image.

19

(a) Luminescence ratio image

y=0   y=110

— : Smoothed data
- - -: Raw data
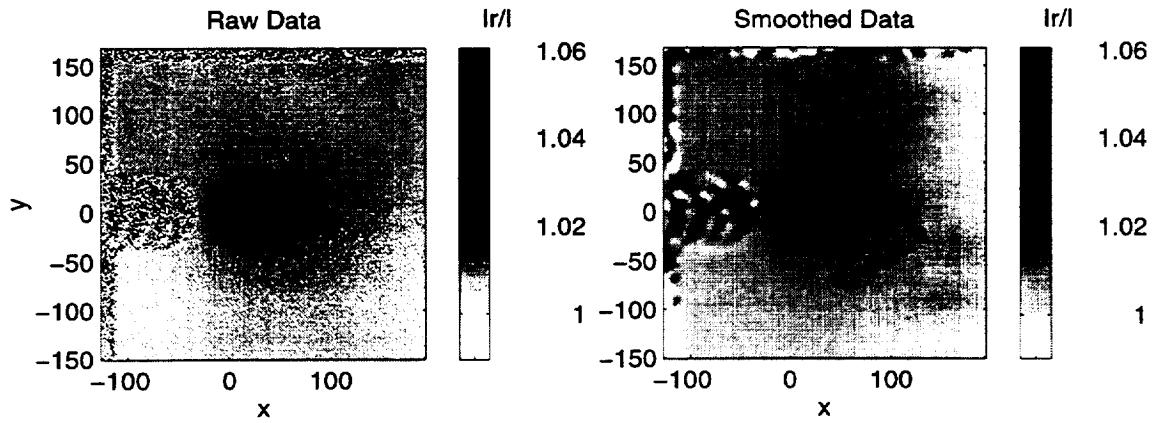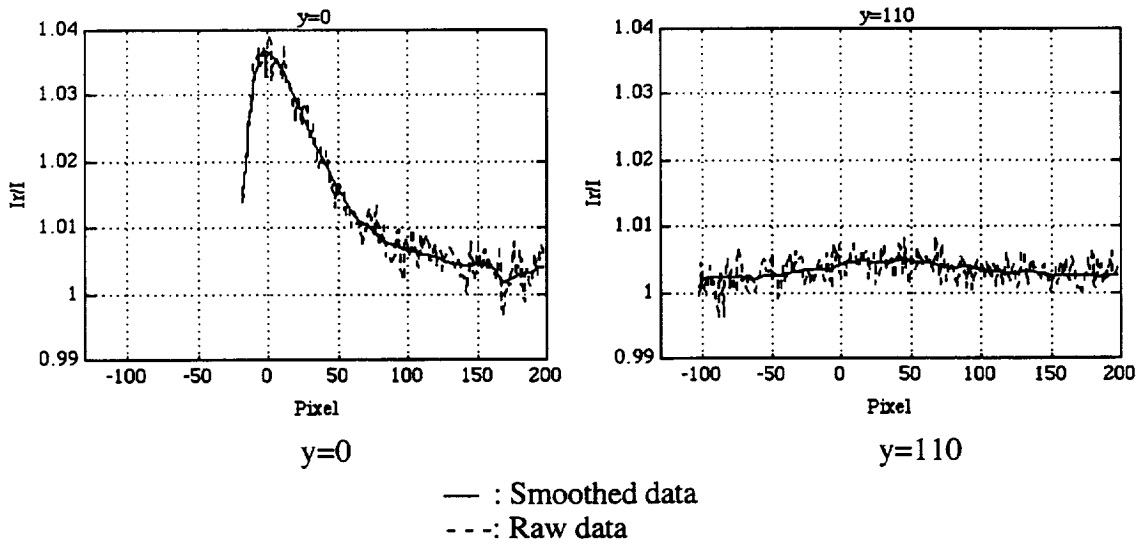
(b) Line plots

D=0.298", r/D=2, Pmax=1.8 psi, θ=45 deg

Figure 3.2.3 Smoothing effects

20

(3) Paint calibration

In this experiment, only the in-situ calibration was applied to avoid any effect of temperature dependency and paint degradation. There were 30 pressure taps within the painted area and the average value of 3x3 pixels square shape corresponding to the pressure tap locations were picked out from the smoothed final luminescence ratio image. Figure 3.2.4 shows the relation between the luminescence ratio (Ir/I) and pressure ratio (P/Pref) at 30 pressure tap locations for Case38 in Table 3.1.1, with the following jet blowing conditions:

Jet nozzle diameter	$D = 0.298"$
Jet nozzle location	$r/D = 2.0$
Maximum pressure	$Pmax = 1.8$ psi
Jet impinging angle	$\theta = 45$ deg

In the figure, Pmax=1.8 psi roughly corresponds to (P/Pref)=1.12. Although there is a liner relation between them according to the theory derived in Chapter 2, there are two distinct linear regions, a larger inclination around (P/Pref)=1 and a smaller inclination in the higher pressure region. There might be some temperature effect because the blowing air was not necessarily at the same temperature as the reference condition. Another possibility is that there might be a nonuniform temperature distribution generated by the impinging jet, as shown in Ref. 10. If the temperature of the higher pressure region where the jet is really impinging is lower than the reference, both the oxygen diffusion and quenching are suppressed and luminescence of the paint increases, which leads to a lower luminescence ratio (Ir/I). But the same tendency was also found in the low-speed wind tunnel tests described later in Chapter 4 and it has probably not been reported previously because this paint has been almost exclusively used in high-speed flows where a single linear relation is obtained.

Because one of the big advantages of the pressure sensitive technique is the reduced number of pressure taps required for the pressure measurements, only five (out of the 30) pressure tap locations were chosen for use in the in-situ calibration. The pressure tap locations selected for calibration were located in the vicinity of the maximum pressure region on the plate and they are shown in Figure 3.2.5.
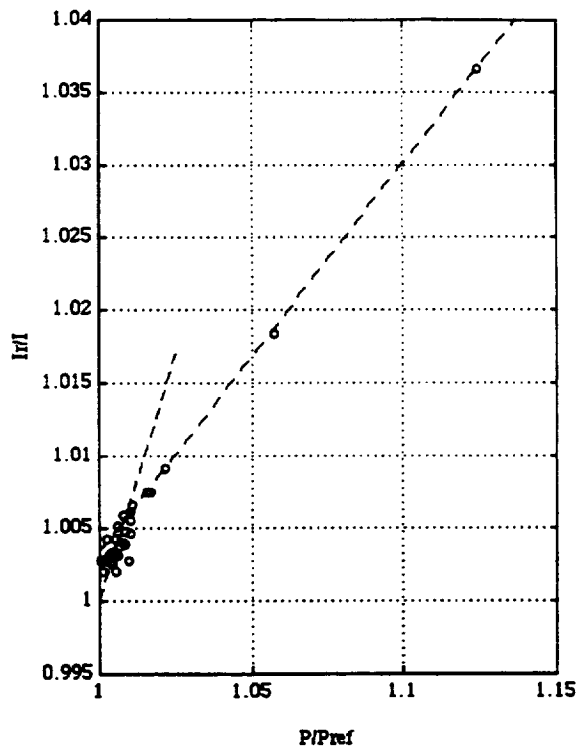
21

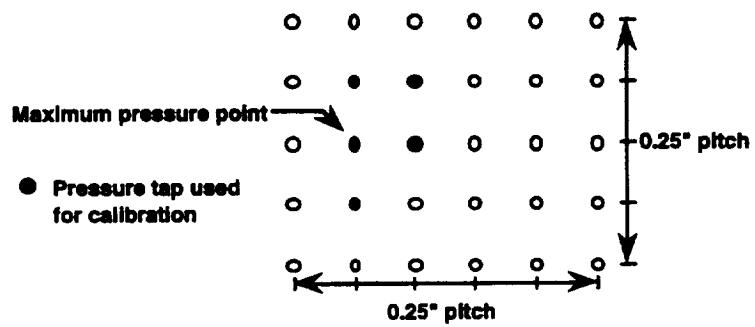Figure 3.2.4 Example of the relation between the luminescence ratio and pressure ratio

Figure 3.2.5 Pressure taps used for calibration

A new algorithm was developed to deal with this two-line calibration instead of the theoretical single line. The algorithm assumes the calibration goes through the point (Ir/I, P/Pref)=(1,1) following the theory, and arranges the six sets of (Ir/I, P/Pref) in ascending order of the pressure ratio

$$[1,1], \ [(Ir/I)_1, \ (P/Pref)_1], \ \cdots \ ,[(Ir/I)_5, \ (P/Pref)_5]$$

where,

$$1 < (I/Ir)_1 < (I/Ir)_2 < (I/Ir)_3 < (I/Ir)_4 < (I/Ir)_5$$

Then, divide those six points into two groups:

$$[0,0] \sim [(Ir/I)_j, \ (P/Pref)_j] : 1 \leq j \leq 4$$

$$[(Ir/I)_{j+1}, \ (P/Pref)_{j+1}] \sim [(Ir/I)_5, \ (P/Pref)_5] : 1 \leq j \leq 4$$

and apply the least square method to determine the two lines:

$$(Ir/I) = A_{1j} + B_{1j} \ (P/Pref) \tag{3.2.1}$$

$$(Ir/I) = A_{2j} + B_{2j} \ (P/Pref) \tag{3.2.2}$$

where when j=4, only a single line calibration is considered and,

$$A_{1j} = A_{2j} \ \text{and} \ B_{1j} = B_{2j}$$

Then, the total error for the pressure estimation is given by:

$$Error_j = \sum_{k=1}^{j} \left\{ \frac{(Ir/I)_k - A_{1j}}{B_{1j}} - (P/Pref)_k \right\}^2 + \sum_{k=j+1}^{5} \left\{ \frac{(Ir/I)_k - A_{2j}}{B_{2j}} - (P/Pref)_k \right\}^2 \tag{3.2.3}$$

The error is computed for each j and the value which minimized the error is selected. In case the two-line calibration is applied, the intersection point of the two lines [(Ir/I)_c, (P/Pref)_c] is also computed.

Finally, the pressure at every point is computed for the two-line calibration by:

$$P = \frac{(Ir/I) - A_{1j}}{B_{1j}} Pref \ \text{for} \ (Ir/I) < (Ir/I)_c \tag{3.2.4}$$

$$P = \frac{(Ir/I) - A_{2j}}{B_{2j}} Pref \ \text{for} \ (Ir/I) \geq (Ir/I)_c \tag{3.2.5}$$

and for the single line calibration by:

$$P = \frac{(Ir/I) - A_{1j}}{B_{1j}} Pref \ \text{for all} \ (Ir/I) \tag{3.2.6}$$

Figure 3.2.6 shows the result of the five point calibration applied to the same case as before and it shows that the two-line calibration agrees well with the data from the other pressure tap locations. In this case, the calibration results using five points are,

$$(Ir/I) = 0.3232 + 0.6769 \ (P/Pref) \qquad \text{for } (Ir/I) < 1.0056 \qquad (3.2.7)$$

$$(Ir/I) = 0.7365 + 0.2669 \ (P/Pref) \qquad \text{for } (Ir/I) > 1.0056 \qquad (3.2.8)$$

and the intersection pressure ratio $(P/Pref)_c$ is 1.0081.

They are very close to the calibration results computed using all of 30 points in the same algorithm, which are given by:

$$(Ir/I) = 0.3743 + 0.6258 \ (P/Pref) \qquad \text{for } (Ir/I) < 1.0057$$

$$(Ir/I) = 0.7361 + 0.2673 \ (P/Pref) \qquad \text{for } (Ir/I) > 1.0057$$

$$(P/Pref)_c = 1.0088$$

These two calibration results overlaps each other in Figure 3.2.6 (b).

In case this calibration with five pressure tap data did not work well, the same method was applied to all 30 pressure taps. The test cases where 30 points data were used in the calibration are indicated by # symbol in Table 3.3.1.
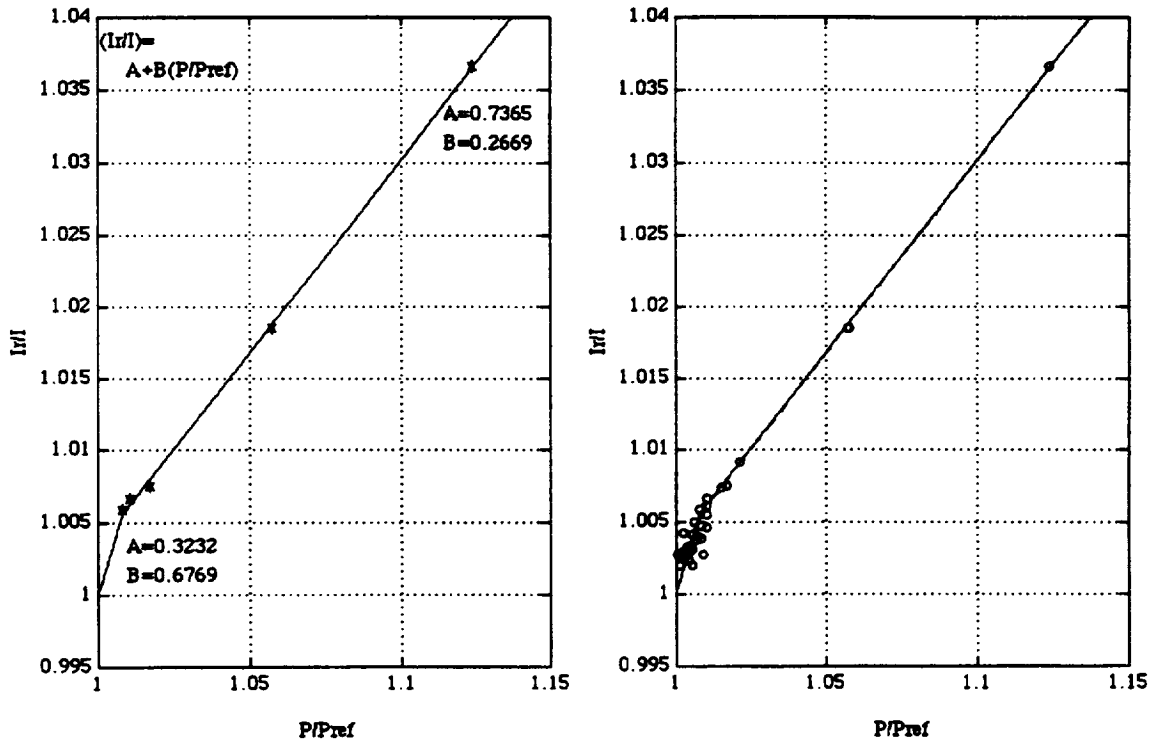
(a) Two-line calibration and five points   (b) Comparison with 30 points

Figure 3.2.6 Typical paint calibration results

3.3 Measurement Accuracy

(1) Overall accuracy and repeatability

The pressure sensitive paint results were compared with the conventional pressure tap measurements to check the overall measurement accuracy. Furthermore, two pressure sensitive paint results tested at the same conditions at different times were compared to check the repeatability of the measurement. The test cases compared were Case38 and Case43 in Table 3.1.1, with the following jet blowing conditions:

Jet nozzle diameter $D = 0.298"$

Jet nozzle location $r/D = 2.0$

Maximum pressure $Pmax = 1.8$ psi

Jet impinging angle $\theta = 45$ deg

Figure 3.3.1 shows a very good agreement among the pressure distribution on the flat plate generated by interpolating 120 pressure tap data within the image (Top) and a corresponding pressure sensitive paint result for Case38 (Middle) and Case43 (Bottom), respectively. The detailed comparison is shown in Figure 3.3.2 along the line, $y/D=0$ (center line) and $y/D=1.2$ (near top edge). Two pressure sensitive paint measurements denoted by the solid line and the dashed line in Figure 3.3.2 agree well and the agreement with the pressure tap data indicated by the symbols is also very good, both in the high and low pressure regions.

The difference between the pressure sensitive paint measurement and the pressure tap measurement defined by:

$$dp = \text{(Pressure sensitive paint result)} - \text{(Pressure tap result)}$$

is computed at 1441 pressure tap locations for 10 cases and plotted in Figure 3.3.3 as a histogram. The result shows that about 70% of the data is within ±0.02 psi and 98.5% is within ±0.1 psi.

25
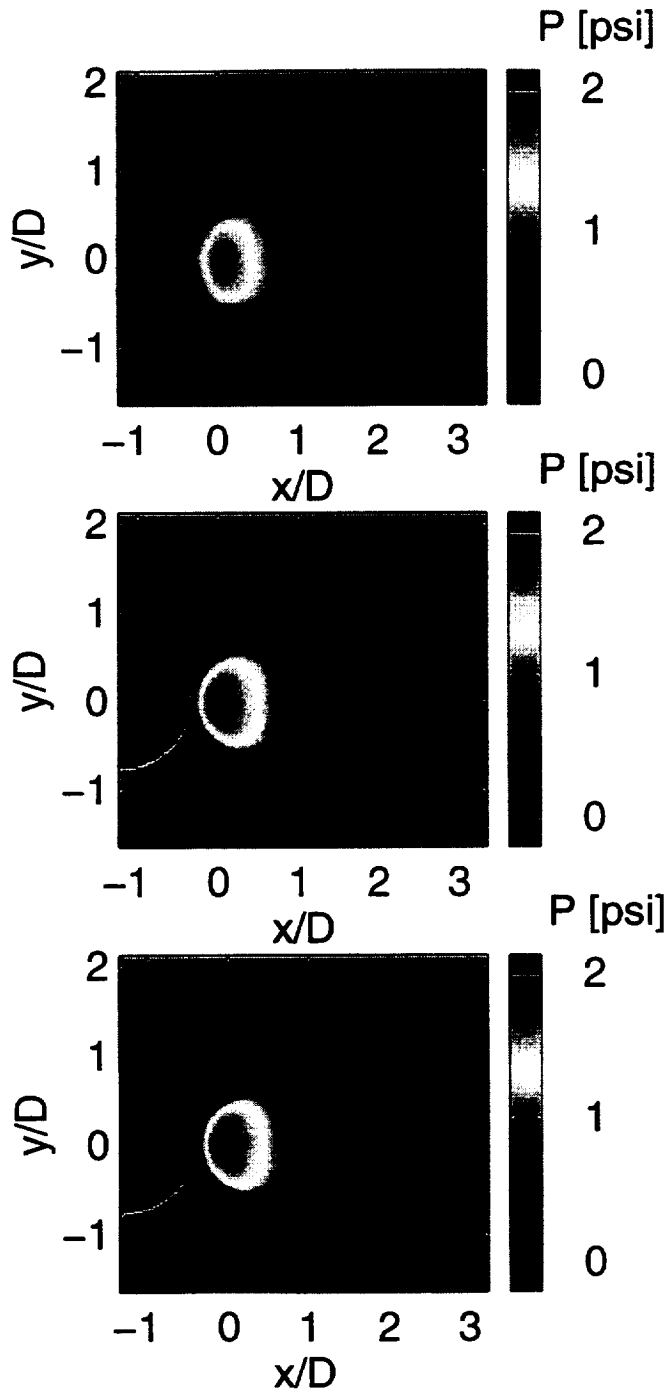
D=0.298", r/D=2, Pmax=1.8 psi, θ=45 deg

Top   Pressure tap measurements
Middle   Pressure sensitive paint (Case38)
Bottom   Pressure sensitive paint (Case43)

Figure 3.3.1 Measurement accuracy and repeatability (Whole pressure field)
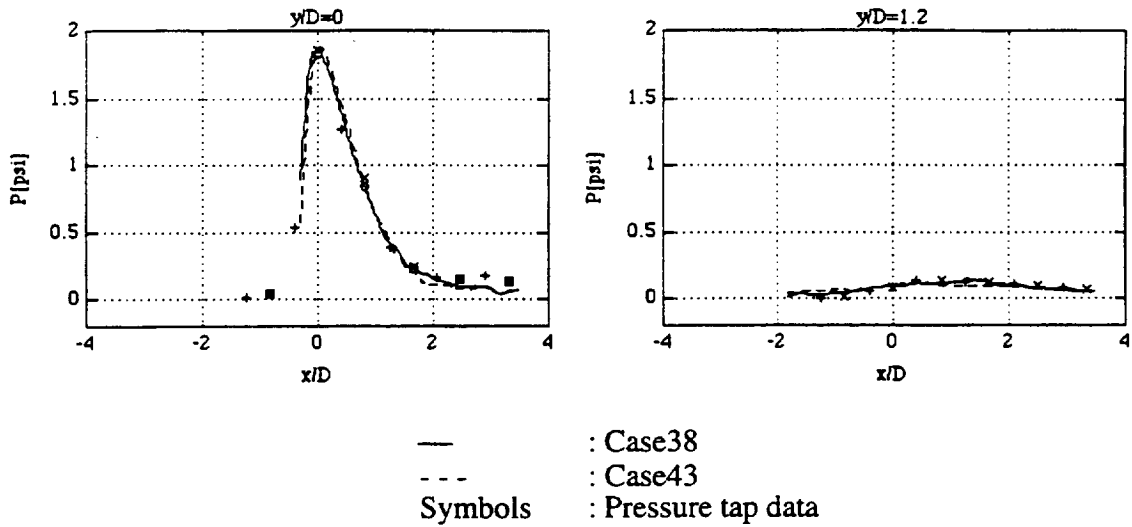
Figure 3.3.2 Measurement accuracy and repeatability (Line plots)

—	: Case38
- - -	: Case43
Symbols	: Pressure tap data
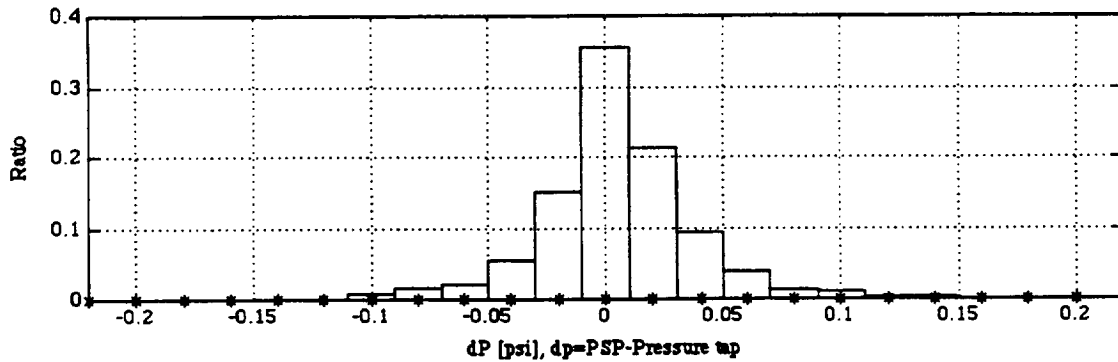
Figure 3.3.3 Overall measurement accuracy

(2) Camera and light source location effects

The pressure sensitive paint measurement was conducted for the same jet blowing conditions with different CCD camera and light source locations. For the jet blowing conditions of D=0.298", r/D=2, θ=45 deg and Pmax=1.4 psi, both the camera and the light source were located normal to the flat plate in Case64 and they were located at around a 45 deg angle from the flat plate in Case93. The pressure distribution along

27

y/D=0 and y/D=1.2 are shown in Figure 3.3.4 and it is found that the camera and the UV light source location had a slight effect on the pressure measurements. The other error sources are evaluated in the next section.
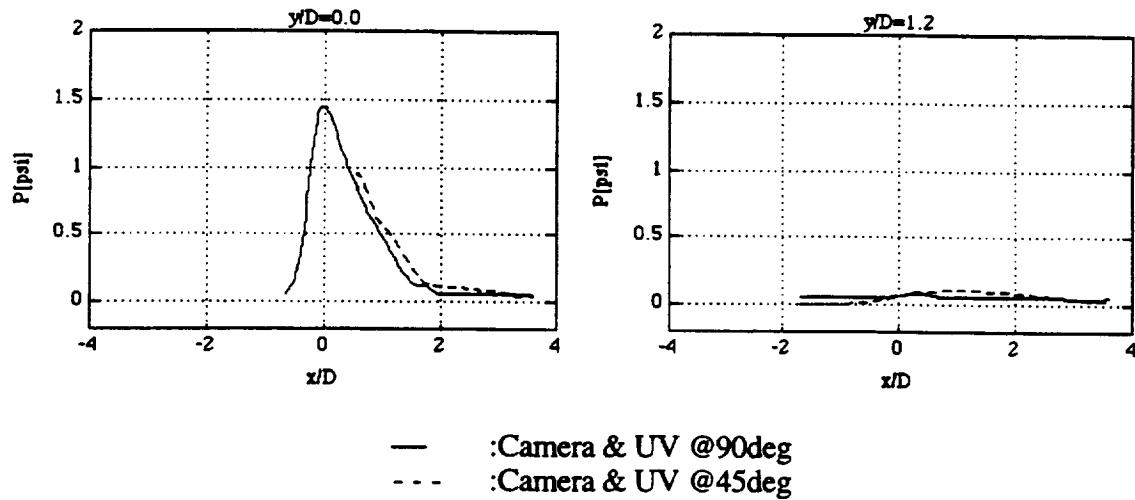
Figure 3.3.4 Camera and UV light source location effects

(3) Error sources

There are a lot of factors which affect the overall measurement accuracy of the pressure sensitive paint and some of them are listed below for further evaluation.

- Light intensity resolution of the CCD camera
- Shot noise of the CCD camera
- Pressure tap measurement
- Temperature

(A) Light intensity resolution of the CCD camera

The light intensity resolution of the CCD camera used in this experiment is limited to 8 bits and it means that the complete dark to complete bright conditions are divided into only 256 discrete values. Table 3.3.1 shows some typical pressure sensitive paint data at sample points in the high and low pressure regions in Case38 described before.

Allowing a 1 count change in any one of the dark, no-wind or on-wind image, the resulting pressure change was computed using the two-line calibration given in Eqs. (3.2 7) and (3.2.8). There is about a 0.3 psi pressure change in the high pressure region and a 0.1 psi in the low pressure region. As a worst case scenario, in case all of the three images change in a direction where the error increases, the error goes up to 0.56 psi and 0.22 psi, respectively. The higher the pressure is, lower the luminescence, and this leads to a smaller denominator of the luminescence ratio. Therefore, one count of uncertainty generates a greater error in the high pressure region. Although the averaging process relaxes the low resolution of the CCD camera, more light intensity resolution is required for more accuracy and Ref. 6 suggests that at least a 12 bit resolution is desirable for a quantitative pressure measurement.

Table 3.3.1 Light intensity resolution effects of the 8 bit CCD camera

Location x/D	0.4100	2.0800
Location y/D	0.0000	2.1000
Pressure by tap [psi]	0.8468	0.0000
Luminescence @ Dark	16.5625	17.5000
Luminescence @ Initial	217.6250	220.4375
Luminescence @ Final	221.4375	222.8125
Luminescence @ No-wind	219.5313	221.6250
Luminescence @ On-wind	213.6875	221.4375
Raw Ir/I	1.0296	1.0009
Ir/I if (Dark+1)	1.0298	1.0009
Ir/I if (Dark-1)	1.0295	1.0009
Ir/I if (No-wind+1)	1.0347	1.0058
Ir/I if (No-wind-1)	1.0246	0.9960
Ir/I if (On-wind+1)	1.0244	0.9960
Ir/I if (On-wind-1)	1.0349	1.0059
Ir/I if (No-wind+1)& (On-wind-1)&(dark-1)	1.0398	1.0107
dP if (Dark+1) [psi]	0.0084	0.0001
dP if (Dark-1) [psi]	-0.0083	-0.0001
dP if (No-wind+1) [psi]	0.2823	0.1076
dP if (No-wind-1) [psi]	-0.2823	-0.1076
dP if (On-wind+1) [psi]	-0.2892	-0.1072
dP if (On-wind-1) [psi]	0.2922	0.1082
dP if (No-wind+1)& (On-wind-1)&(dark-1) [psi]	0.5647	0.2152

(B) Shot noise of the CCD camera

The shot noise of the CCD camera is characterized by the full well depth, Nmax, which represents the maximum number of electrons counted in each pixel. According to Ref. 6, the pressure resolution ε_p is approximately given by:

$$\frac{\varepsilon_p}{P} \approx \frac{2}{\sqrt{Nmax}}$$

For a typical value of Nmax=50,000 and atmospheric pressure P=1atm=14.695 psi,

$$\frac{\varepsilon_p}{P} \approx 0.003 \Rightarrow \varepsilon_p = 0.044psi$$

is the error due to the shot noise. Although this is rather large compared to the overall measurement accuracy, the shot noise effect is also minimized by the averaging process.

(C) Pressure tap measurement

Generally, a typical overall accuracy of the pressure transducer measurement is about 0.5% of the full scale. For the pressure transducer used in this experiment with a 2.5 psi capacity, the error is:

$$\Delta Ptap=2.5 \text{ psi} \times 0.005 = 0.0125 \text{ psi}$$

Under the reference pressure condition of Pref=1atm=14.695 psi for calibration, the error introduced by the pressure transducer is,

$$(\Delta Ptap/Pref) = 0.0125 \text{ psi} / 14.695 \text{ psi} = 8.5 \times 10^{-4}$$

and this is very small compared to the scale used in the calibration.

(D) Temperature effect

As described above in Chapter 2, the basic relation between the luminescence ratio and pressure ratio is given by Eq.(2.2.12) to Eq.(2.2.14) when the temperature is constant between the no-wind and on-wind conditions. But if no-wind images are taken at temperature, T, and on-wind images are taken at temperature, T', Eq.(2.2.8) yields:

$$\frac{I_0(T')/I(P,T')}{I_0(T)/I_r(Pref,T)} = \frac{1+a(T')P}{1+a(T)Pref} \tag{3.3.1}$$

and therefore,

$$\frac{Ir(Pref,T)}{I(P,T')} = \frac{Io(T)}{Io(T')} \left[\frac{1}{1+a(T)Pref} + \frac{a(T')Pref}{1+a(T)Pref} \left(\frac{P}{Pref} \right) \right]$$

$$= \frac{Io(T)}{Io(T')} \left[A(T) + \frac{a(T')}{a(T)} B(T) \left(\frac{P}{Pref} \right) \right]$$

$$= A'(T') + B'(T') \left(\frac{P}{Pref} \right) \qquad (3.3.2)$$

where,

$$A'(T') = \frac{Io(T)}{Io(T')} A(T) \qquad (3.3.3)$$

$$B'(T') = \frac{Io(T)}{Io(T')} \frac{a(T')}{a(T)} B(T) \qquad (3.3.4)$$

Figure 3.3.5 from Ref. 2 shows the result of an a priori calibration for the PtOEP/GP-197 mixed using the same recipe as in this study under the reference conditions of T=25°C and Pref=175 mmHg. From this figure, $I_0(T)/I_0(T')$ and a(T') can be computed using Eqs. (2.2.13),(3.3.3) and (3.3.4) as shown in Table 3.3.2 and the temperature dependency of these two values is plotted in Figure 3.3.6.

To estimate the temperature effect in the present impinging jet experiment from these data, first the reference condition is adjusted to the typical impinging jet measurements condition T_0=23°C , Pref=1atm, which yields:

$$A(To) = \frac{1}{1+a(To)Pref} = 0.3668$$

$$B(To) = \frac{a(To)Pref}{1+a(To)Pref} = 0.6332$$

where,

$$a(T_0) = 0.002271$$

is determined from Figure 3.3.6. These values are close to the lower pressure region of the two-line calibration given by Eq.(3.2.7).

Assuming the on-wind images are taken at T'=22, 23 and 24°C, then the luminescence ratio at typical high and low pressure regions based on the calibration constants computed above are shown in Table 3.3.3.
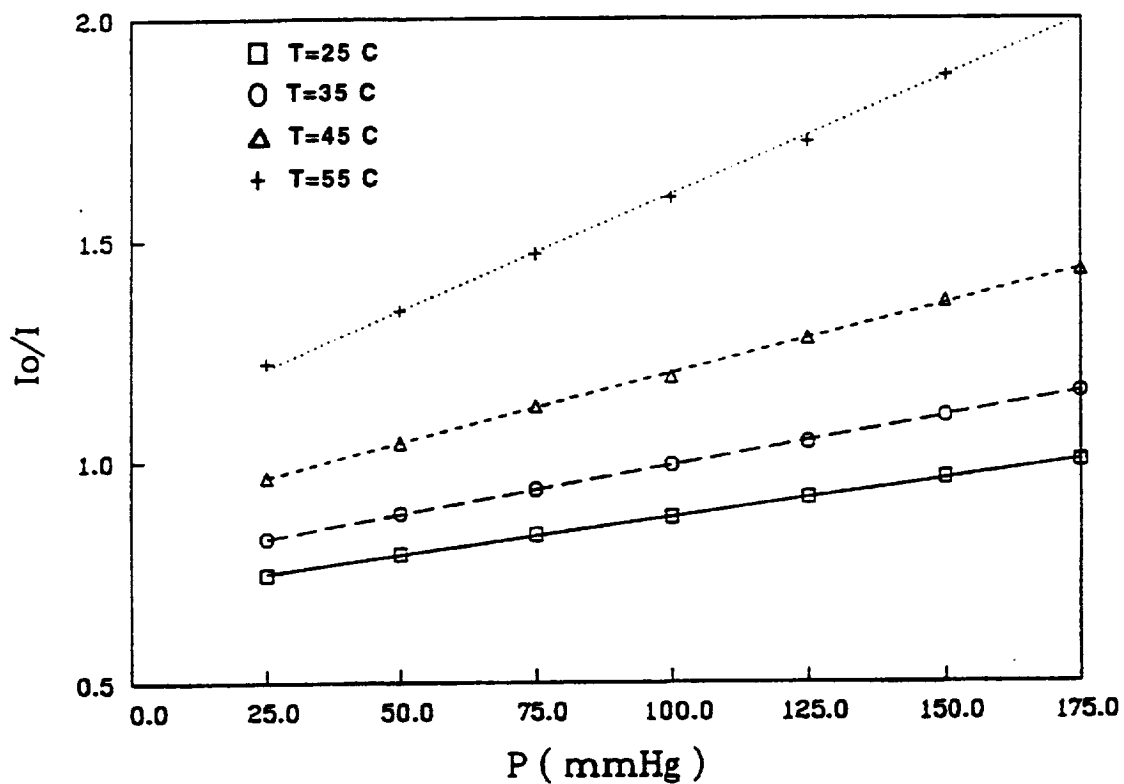
31

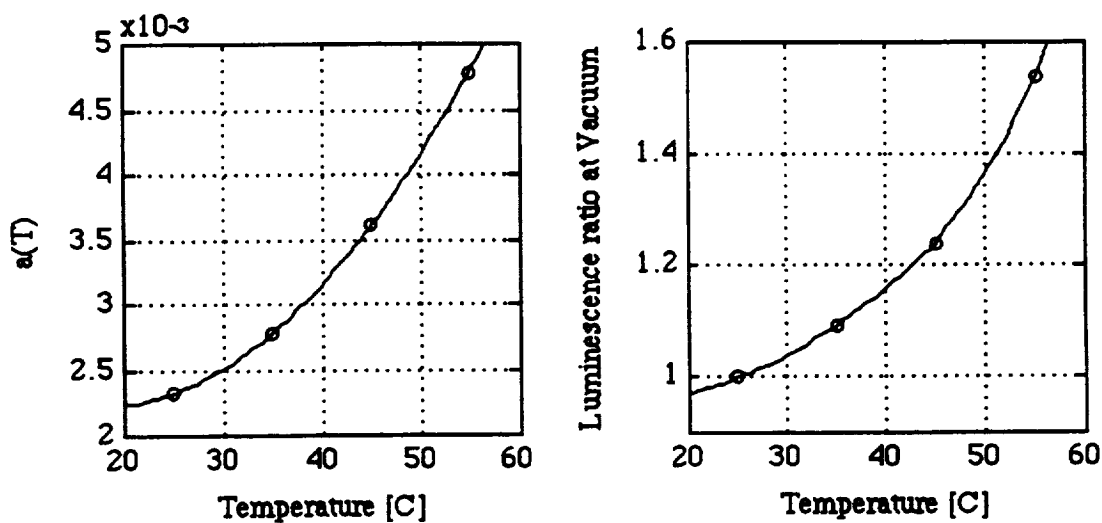Figure 3.3.5 Calibration result of PtOEP/GP-197 at different temperatures(Ref. 2)

Figure 3.3.6 Temperature dependency of the Stern-Volmer coefficient
and luminescence ratio at vacuum

32

Table 3.3.2 Temperature effects on the paint calibration

T' [°C]	A'(T')	B'(T')	a(T')[1/mmHg]	$I_0(T=25°C)/I_0(T')$
25	0.7095	0.2905	0.002340	1.000
35	0.7760	0.3780	0.002784	1.0937
45	0.8805	0.5565	0.003612	1.2410
55	1.0918	0.9114	0.004774	1.5388

Table 3.3.3 On-wind temperature effects

	23 °C	23 °C	23 °C
No-wind Temperature T_0			
On-wind Temperature T'	22 °C	23 °C	24 °C
Stern-Volmer Coefficient a(T')	0.00224	0.00227	0.00231
Vacuum luminescence ratio I_0 (T=25°C)/I_0(T')	0.9824	0.9882	0.9941
Ir/I @ P=0.1 psi	1.00261	1.00431	1.00895
[(Ir/I)T']-[(Ir/I)T'=23] @ P=0.1 psi	-0.0017	0	0.00464
dP [psi] @ P=0.1 psi	-0.037	0	0.101
Ir/I @ P=1.8 psi	1.07542	1.07756	1.08299
[(Ir/I)T']-[(Ir/I)T'=23] @ P=1.8 psi	-0.0021	0	0.00543
dP [psi] @ P=1.8 psi	-0.119	0	0.302

From the table, only a 1°C temperature change between the no-wind and on-wind conditions causes about a 0.002 - 0.005 change in luminescence ratio, which correspond to at most 0.3 psi pressure difference for the calibration constants given by Eqs. (3.2.7) and (3.2.8) in Case38.

(E) Summary

Each error source, except the pressure transducer, has a potential for more than 0.1 psi error in pressure measurement. The data reduction process, such as an averaging and a smoothing reduce these errors and finally the overall measurement accuracy of 0.1 psi was achieved in this experiment.

3.4 Parametric Study

To demonstrate the static pressure measurement capability and its advantages, the pressure sensitive paint was applied to a series of parametric studies by varying the jet blowing conditions. In this study, only one parameter was changed at a time and everything else was held constant. The parameters used were as follows and the bold-face conditions were used as the baseline conditions.

Jet nozzle location   r/D = 1.08, **2**, 4

Maximum pressure   Pmax = 1.0, **1.4**, 1.8 psi

Jet impinging angle   θ = 22.5, **45**, 67.5, 90 deg

(1) Maximum pressure effects

The effects of the maximum pressure on the flat plate are shown in Figure 3.4.1 with the maximum pressure on the plate varying among Pmax=1.0 psi (Case52), Pmax=1.4 psi (Case50) and Pmax=1.8 psi (Case38) with the other parameters fixed at the baseline values. On the left hand side, the pressure is displayed as the physical value and the difference in magnitude of the pressure is obvious. However, on the right hand side, the pressure is nondimensionalized by the maximum pressure, Pmax, and it is easy to see the pressure fields are similar among these three conditions and that no higher-order effects are apparent.

(2) Nozzle diameter effects

The effects of the nozzle diameter are shown in Figure 3.4.2 with the diameter varying between D=0.298" (Case38) and D=0.155" (Case66), with Pmax=1.8 psi and the other parameters fixed at the baseline values. Although the pressure fields in the upper figure look completely different when they are displayed by physical location and pressure, these two pressure fields are found to be very similar after the horizontal and vertical positions were nondimensionalized by the nozzle diameter, and the pressure was nondimensionalized by the maximum pressure (Pmax) on the plate. In the conventional pressure tap measurements in which the pressures are measured at fixed points, it is hard to maintain the same spatial resolution of the measurement in a case like the present one. But for the pressure sensitive paint, pressure data are available everywhere and a coarse

interpolation is not necessary. This is one of the advantages of the pressure sensitive paint technique as a continuous pressure field measurement.

(3) Jet impinging angle effects

The effects of the jet impinging angle are shown in Figure 3.4.3 with the angle varying among θ=22.5 deg (Case86), 45 deg (Case93), 67.5 deg (Case102) and 90 deg (Case109) with the other parameters fixed at the baseline values. As the impinging angle increases, the positive pressure region changes from an elliptic shape to a circular in the x (lateral) direction and the higher pressure region spreads in the y (vertical) direction. From the pressure tap results at θ=22.5 deg, there was a negative pressure region around x/D=-0.5, y/D=0. This negative pressure region was generated by the flow entraining into the jet from the near surface region. In the pressure sensitive paint data, this region is not clear because the paint is calibrated only in the positive pressure range and the measurement accuracy is therefore not so good in the negative pressure region.

(4) Nozzle location effects

The nozzle location effects are shown in Figure 3.4.4 with the location varying among r/D=1.08 (Case95), r/D=2 (Case93) and r/D=4 (Case36) with the other parameters fixed at the baseline values. As the nozzle location become farther from the flat plate, the region affected by the jet become larger and the pressure gradient on the plate become milder, as the jet expands and entrains more air from the surrounding atmosphere.
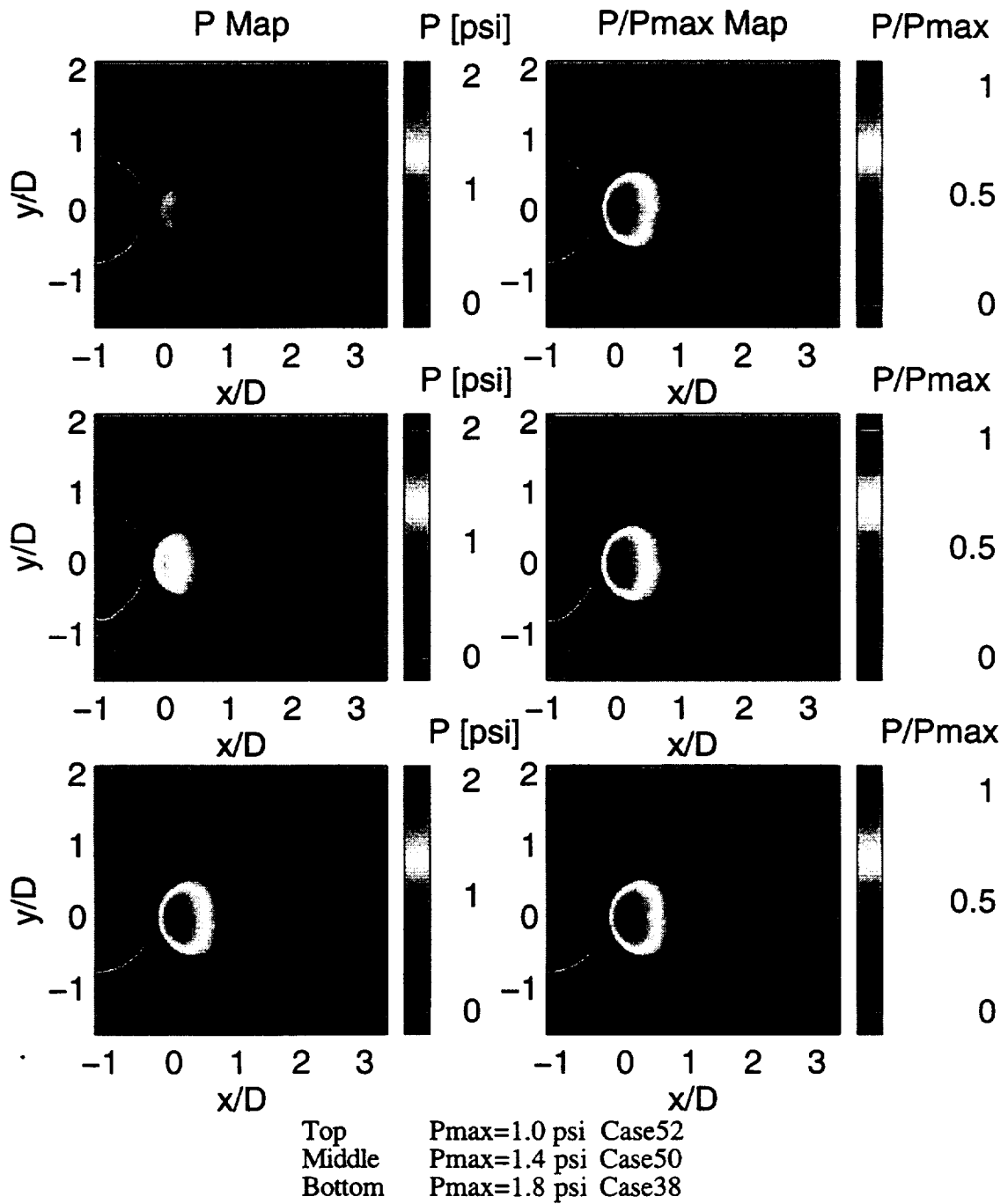
Figure 3.4.1 Parametric study — Maximum pressure effects

Top	Pmax=1.0 psi	Case52
Middle	Pmax=1.4 psi	Case50
Bottom	Pmax=1.8 psi	Case38

Left	D=0.298"	Case38
Right	D=0.155"	Case66
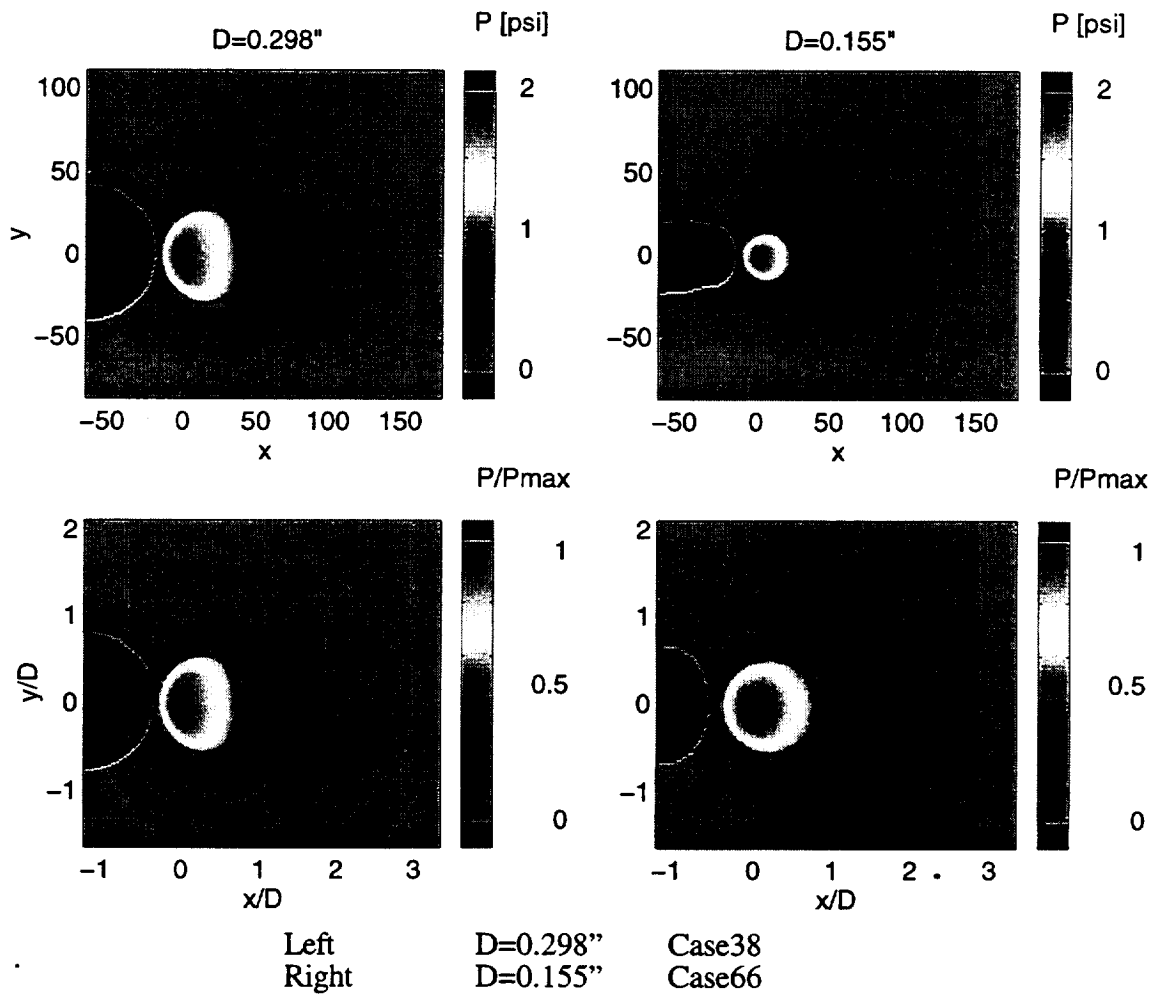
Figure 3.4.2 Parametric study — Nozzle diameter effects
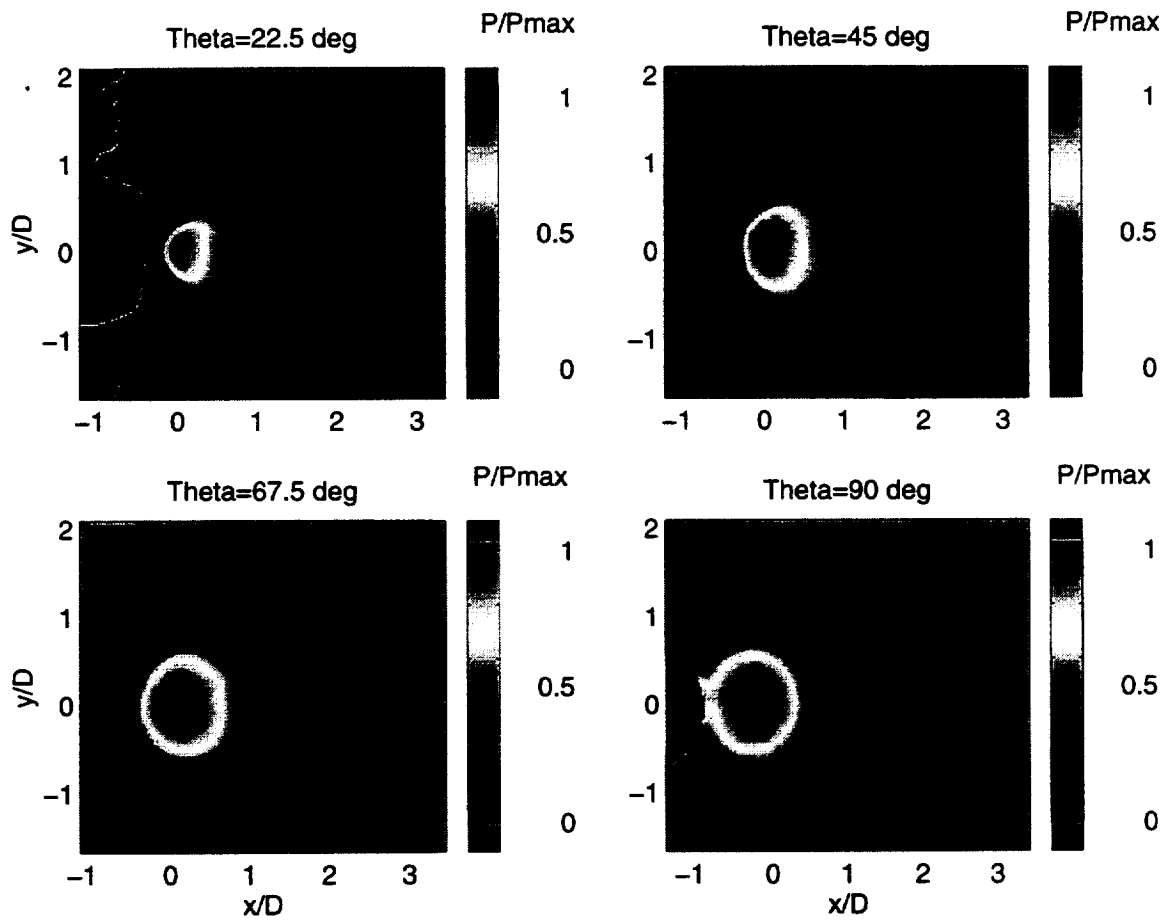
Top left	θ=22.5 deg	Case86
Top right	θ=45.0 deg	Case93
Bottom left	θ=67.5 deg	Case102
Bottom right	θ=90.0 deg	Case109

Figure 3.4.3 Parametric study — Impinging angle effects

Top	r/D=1.08	Case95
Middle	r/D=2	Case93
Bottom	r/D=4	Case36
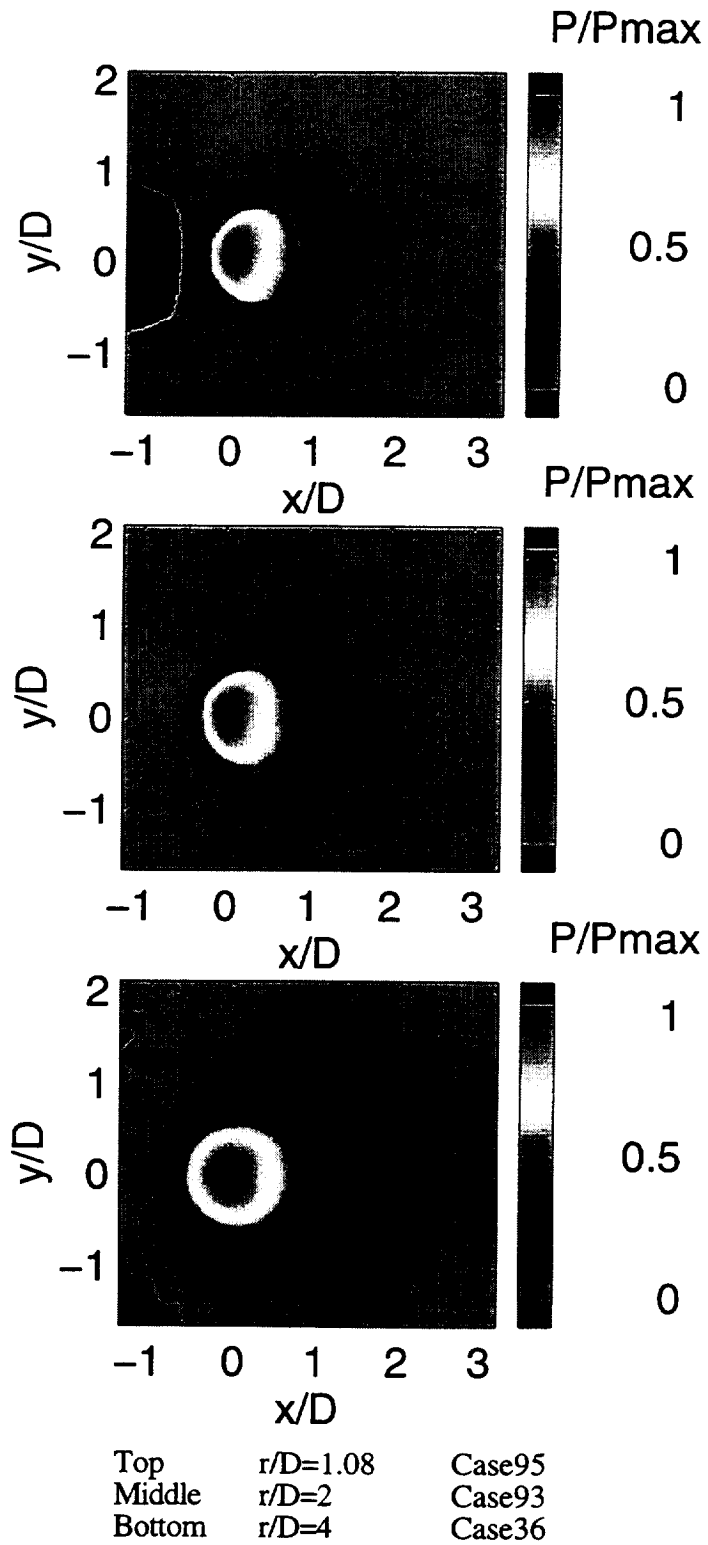
Figure 3.4.4 Parametric study — Nozzle location effects

Chapter 4   Low-Speed Wind Tunnel Tests

Low-speed wind tunnel tests were conducted to demonstrate the pressure sensitive paint technique at low speed and to investigate the vortical flow field over a delta wing. The technical problems encountered in low-speed testing were resolved by using a high resolution CCD camera and applying proper corrections to the image data based on the experience from the previous impinging jet measurements.

4.1 Experimental Set-up

A schematic of the experimental set-up is shown in Figure 4.1.1. The experiment was conducted in the subsonic wind tunnel located in the Department of Aeronautics and Astronautics at Stanford University. This is a closed-circuit wind tunnel and the test section is 18" x 18" (0.45m x 0.45m) in cross-section and 34" (0.86m) in length. Although all the walls of the test section were made of Plexi Glas, a portion of the ceiling was replaced by a 1/8" thickness normal glass to avoid the absorption of UV light and red light emitted from the paint.
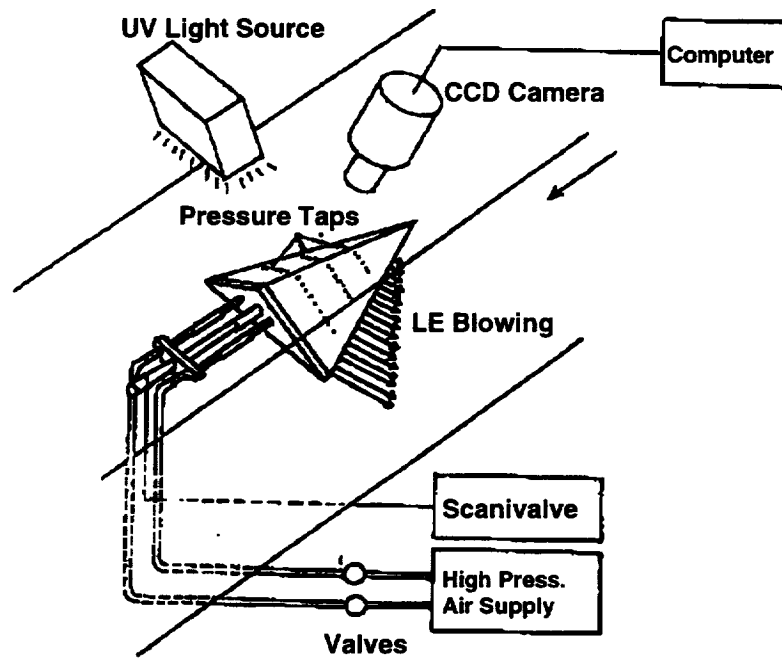
(a) Schematic
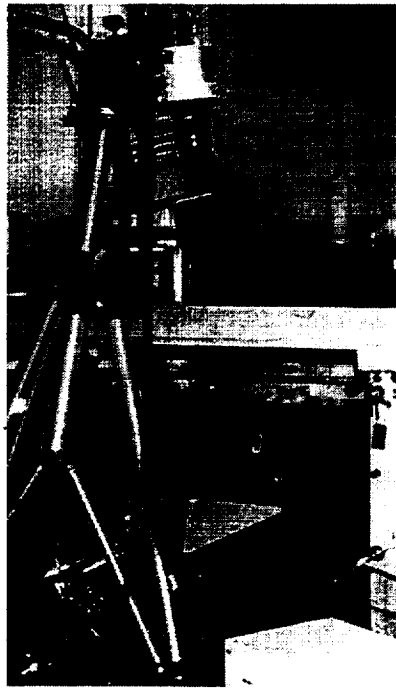
(b)Photo

Figure 4.1.1 Experimental set-up for the low-speed wind tunnel tests

60deg

0.685C
0.542C
0.397C

C=7.552 inch

Pressure Tap Row 1
(5 on each side)
Pressure Tap Row 2
(8 on eqach side)
Pressure Tap Row 3
(9 on each side)

b=8 inch

0.002" width
(t/c=0.00026)
x/c=0.078

Slot

0.025" width
(t/c=0.0033)
x/c=0.917

s=0

1.881 inch

s=Smax
s
12.3 deg
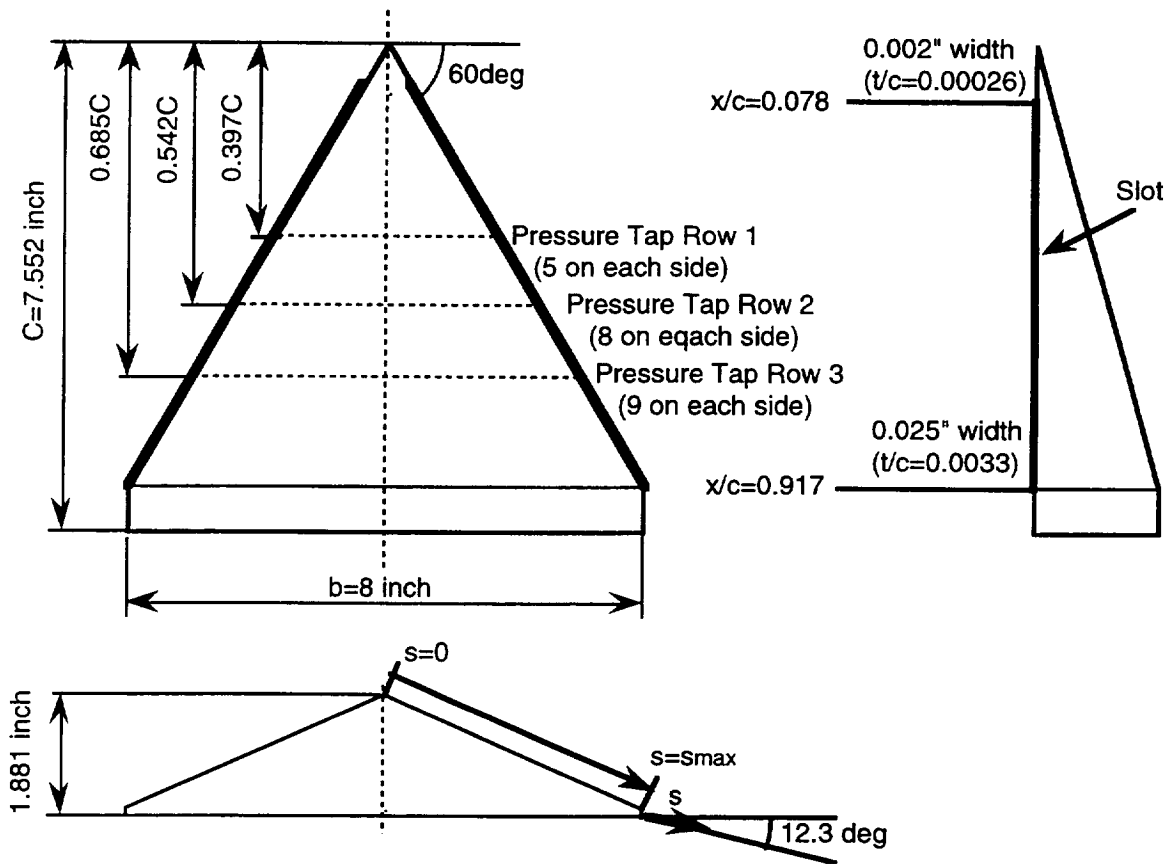
(a) Schematic
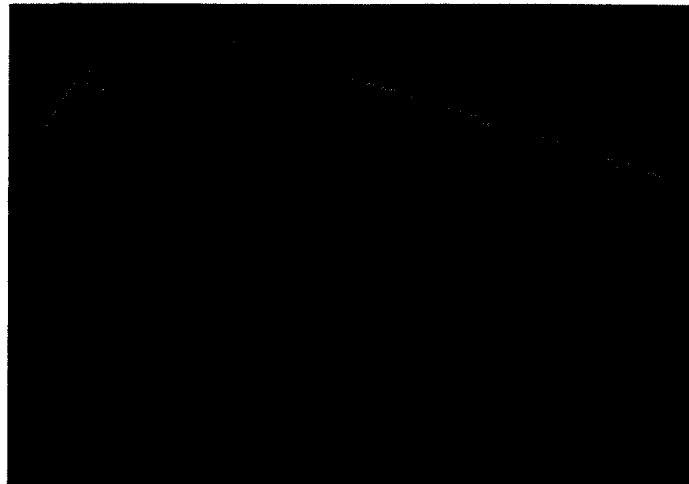
(b) Photo in illuminated condition

Figure 4.1.2 Wind tunnel test model

Figure 4.1.2 illustrates the wind tunnel model and its dimensions. The model was a 60 deg delta wing with leading edge blowing slots on both sides. The blowing slot was directed at an angle of 12.3 degrees downward with respect to the bottom surface of the model and spanned from $x/c=0.078$ to $x/c=0.917$. The slot opening was tapered from 0.0002" $(t/c=0.00026)$ at $x/c=0.078$ to 0.025" $(t/c=0.0033)$ at $x/c=0.917$. The model had a separate plenum chamber on each side and the blowing air was introduced into each chamber through a separate hose from the high pressure supply located outside of the wind tunnel. Therefore, the blowing condition on each side could be controlled independently by adjusting the valves. There were two models of identical geometry, one was a pressure model and another was a visualization model. The pressure model was equipped with 44 pressure taps arranged in three rows for the conventional pressure measurements. These models had been used in previous work by Celik et al. (Ref. 11) to investigate the lift enhancement effect of the leading edge blowing. Force and pressure measurements had been conducted along with the flow visualization using smoke and surface oil flow both, with and without leading edge blowing conditions.

The pressure sensitive paint (PtOEP/GP-197) was air-brushed over a glossy white paint (Krylon 91591) which was applied first on the whole upper surface as an undercoat. The measured typical thickness of the pressure sensitive paint layer was 30μm. A Photometrics 14 bit digital CCD camera borrowed from the Fluid Mechanics laboratory of NASA Ames Research Center was used for the image acquisition to resolve the relatively small luminescence change observed at low speeds. A 50 mm Nikon standard camera lens with a 650 nm bandpass filter was used with the CCD camera. The aperture was set to f=5.6 and the shutter speed was adjusted for each case so that the images were as bright as possible without overloading the CCD. A Pentium 133 Personal Computer was used to control the camera and to store the images for later data reduction. Both the camera and the UV light source were located above the tunnel ceiling so that the UV light for paint illumination went through the glass portion of the ceiling and the emitted red light from the paint was also collected through it. The paint data were acquired on a 510 x 510 pixel array in order to increase the spatial resolution as much as possible. The pressure sensitive paint measurements were mainly focused on the right-hand side of the model only, as it was difficult to adjust the lighting and camera conditions for both of the distinct flat surfaces of the model. Pressure tap data, the plenum chamber pressure of the model (to determine the blowing conditions) and tunnel free-stream conditions were measured by the tunnel measurement system (scanivalve) at the same time as the paint image acquisition.

The test conditions are shown in Table 4.4.1. The uniform flow velocity in the test section was set to 35 m/s for most cases to make the pressure change as large as possible, although a flow velocity of 25 m/s was also used in some restricted cases. The Reynolds number based on the model chord length was 4.6×10^5 and 3.3×10^5, respectively. Three angles of attack ($\alpha = 10$, 20 and 30 deg) were investigated together with two sideslip angles ($\beta = 0$ and 5 deg). Leading edge blowing was applied only on the right-hand side of the model in most cases since the previous work by Celik et al. (Ref. 11) had shown that the vortex flow system on both sides of the wing were completely independent of each other under these test conditions. The blowing conditions were characterized by the momentum coefficient of the jet $C\mu$ defined by:

$$C\mu = \frac{(\rho V_j)V_j A_j}{(1/2)\rho U^2 S}$$

Three blowing conditions were investigated, $C\mu = 0$, 0.03 and 0.06.

As described before, the pressure sensitive paint is also sensitive to temperature. Therefore in this wind tunnel test, on-wind images were taken after running the tunnel for 30 minutes to ensure that thermal equilibrium had been achieved on the model. The temperature in this return-circuit wind tunnel increased appreciably (~5 degrees C) during the initial running after start-up. Then, the no-wind images were taken immediately after the tunnel fan motor was turned off and the free-stream velocity in the test section was near-zero. This was done to minimize the temperature difference of the model surface between on and off wind conditions.

Table 4.1.1 Test cases — Low-speed wind tunnel tests

Alpha [deg]	Beta [deg]	U [m/s]	Cmu Left	Cmu Right	Visualization Model 16 images	48images	Pressure Model 16 images	48 images
10	0	35	0	0		1034	1064	1068
			0	0.03		1031	1062	1066
			0	0.06		1032	1063	1067
10	0	25	0	0				1084
			0	0.03				1082
			0	0.06				1083
10	5	35	0	0				1102
			0	0.03				1098
			0	0.06				1099
			0.03	0				1100
			0.06	0				1101
20	0	35	0	0	1027	1037	1055&1078	1071&1081
			0	0.03	1025	1035	1053	1069&1079
			0	0.06	1026	1036	1054	1070&1080
20	0	25	0	0				1074
			0	0.03				1072
			0	0.06				1073
20	5	35	0	0	1044			1092
			0	0.03	1045			1088
			0	0.06	1046			1089
			0.03	0	1047			1090
			0.06	0	1048			1091
30	0	35	0	0		1030&1043	1058	1077
			0	0.03		1028&1041	1056	1075
			0	0.06		1029&1042	1057	1076
30	0	25	0	0		1040	1061	1087
			0	0.03		1038	1059	1085
			0	0.06		1039	1060	1086
30	5	35	0	0				1097
			0	0.03				1093
			0	0.06				1094
			0.03	0				1095
			0.06	0				1096

4.2 Data Reduction

(1) Sequence

Data reduction of the pressure sensitive paint images was carried out on a Silicon Graphics Indy Workstation using Mathworks MATLAB software. The data reduction was performed in the following sequence, characterized as corrections (steps 1-7) and paint calibration (steps 8-10). It was designed to extract as much accurate quantitative data as possible from these images with relatively low signal-to-noise ratios due to the low testing velocities.

1. Subtract a Dark image (obtained using the same camera settings) from the no-wind and on-wind images to account for the camera dark current noise.
2. Sum up (average) the 48 or 16 images for both of the no-wind and on-wind conditions.
3. Find the model displacement between the on-wind and no-wind images by comparing the leading edge locations. If the model was displaced, apply a flat field correction and adjust the model position in no-wind image.
4. Apply a low-pass filter to both of the summed-up no-wind and on-wind images.
5. Compute the raw luminescence ratio between the low-pass filtered images.
6. Estimate the luminescence ratio at the pressure tap locations and removed pixels such as flawed paints and scratches, from the surrounding points.
7. Apply the low-pass filter again to the raw luminescence ratio image to create the final luminescence ratio data.
8. Plot the luminescence ratio data along the lines corresponding to three pressure tap rows and apply smoothing. Then, pick out the luminescence ratio data at the pressure tap locations.
9. Calibrate the paint using the pressure tap data and the corresponding luminescence ratio data.
10. Apply the calibration to the whole image and make a pressure distribution map.

(2) Corrections

Flat field correction in step 3 was applied to make up the difference in the sensitivity of each pixel of the CCD camera. This correction was necessary only when the model moved between the no-wind and on-wind images because the luminescence of the paint at a particular point on the model was sensed by a different pixel in the camera, possibly with a different sensitivity. In this correction, each of the no-wind and on-wind images was divided by a flat field image, pixel by pixel. The flat field image was generated by summing up 16 images of a uniformly illuminated white field.

Low-pass spatial filtering in steps 4 and 8 was applied to reduce the high spatial frequency component of the images such as spot noise and to compensate for subpixel movement of the model. The low-pass filter used in this data reduction was a simple 9 component average in which the value at one pixel was replaced by the average value of the surrounding 8 pixels and itself. In this process, meaningless data such as the background and the pressure tap locations were omitted from the averaging.

The effects of the corrections up to step 7 were evaluated for a typical case of α=20 deg, β=0 deg, U=35 m/s and no blowing. Figure 4.2.1 shows the luminescence ratio along pressure tap row#1 and its spatial frequency spectrum at different data reduction stages. Even in the first three cases in Figure 4.2.1, data estimation in step 6 were applied to make up the values at the pressure tap locations. Without any corrections and filtering, the data in the top figure are very noisy. Both the flat field/model displacement correction and low-pass filtering work well by themselves by reducing the high spatial frequency component. The whole correction process reduces the noise, especially in the high spatial frequency regions. The effects of the number of images averaged were also evaluated about the same test condition in the same manner. Figure 4.2.2 shows the final luminescence ratio along pressure tap row#3 with the spatial frequency spectrum at 4, 12, 24, 36 and 48 averages. The results show a relatively small effect of the number of images averaged, thus suggesting that, in this particular experiment, the contribution of shot noise of the CCD camera was relatively small compared to the other error sources.

(3) Paint calibration

As shown in Figure 4.2.1, the luminescence ratio along the pressure tap row was not smooth enough, even after the corrections had been applied. Picking out luminescence ratio data for paint calibration seemed to introduce another error source. Therefore, one-dimensional data smoothing was applied to the data in step 8 of the sequence. In this smoothing process, each value in the data was replaced by the average of five values including two forward and two backward values and this sequence was performed 20 times. The effects of this smoothing process are shown in Figure 4.2.3 for pressure tap row#3 at α=20 deg, β=0 deg, U=35 m/s and no blowing. The left-hand side of the figure shows a luminescence ratio along with the data to be picked out for the calibration and the right-hand side of the figure show the relation between the picked-out luminescence ratio and corresponding pressure tap data on the right-hand side of the model. Clearly smoothed data show a more consistent relation between them.

The in-situ calibration was applied using the smoothed paint data and the pressure tap measurements obtained in each case. The paint calibration was conducted separately on the two sides of the model since there was a large difference in the illumination and image taking conditions between the two sides. The transformation from the luminescence ratio data to pressure distribution was also conducted separately for the two sides after locating the center line of the model in each image. Typical calibration results at α=10, 20 and 30

deg without sideslip and blowing at U=35m/s are shown in Figure 4.2.4. In this figure, the horizontal and vertical axes indicate a pressure change from the no-wind condition and the luminescence ratio, respectively and 22 data points at pressure tap locations are plotted for each side of the model. At α=10 deg, the pressure changes from the no-wind condition are very small and the points at each pressure tap location lie almost on a straight line as is described by the theory. But at higher angles of attack, the data in the larger pressure change regions show another line with a smaller inclination than for α=10 deg, as was observed in the previous impinging jet experiments. In this wind tunnel test, this two-line behavior was represented by a quadratic curve instead of the two lines for simplicity and the linear or quadratic relation was applied during the data reduction process depending on the behavior of the data points. In both cases, the mathematical expression of the calibration was determined by the least square approximation.

(4) Light intensity resolution of the CCD camera

The light intensity resolution of the digital CCD camera used in this wind tunnel testing is 14 bits. The complete dark to complete bright conditions are divided into 16,384 discrete values and this is 64 times as many as the 8 bit camera used in the previous impinging jet measurements. A possible measurement error due to the discrete light intensity resolution in a typical case of α=20 deg, β=0 deg, U=35 m/s and no blowing was analyzed in the same manner as Chapter 3.3 and the results are shown in Table 4.2.1. The pressure changed introduced by one count of uncertainty of the light intensity is very small both in high and low suction regions and the advantage of the high grade CCD camera is obvious.
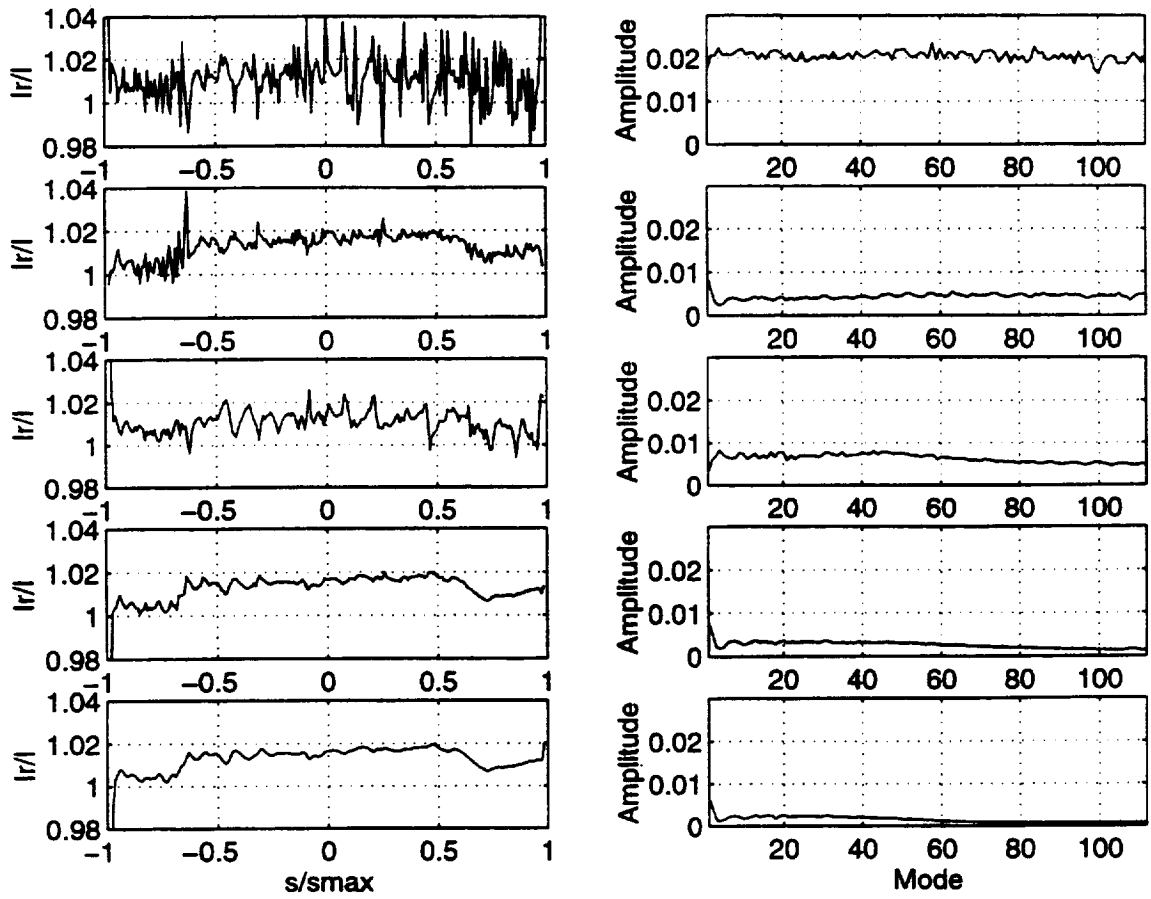
Pressure tap row#1, α=20 deg, β=0 deg, U=35 m/s, Cμ=0

Top	No correction
Second	Only flat field/model displacement correction
Third	Only low-pass filtering to no-wind and on-wind images
Fourth	Flat field/model displacement correction + low-pass filtering
Bottom	Whole corrections (Final luminescence ratio data)

Figure 4.2.1 Correction effects

49
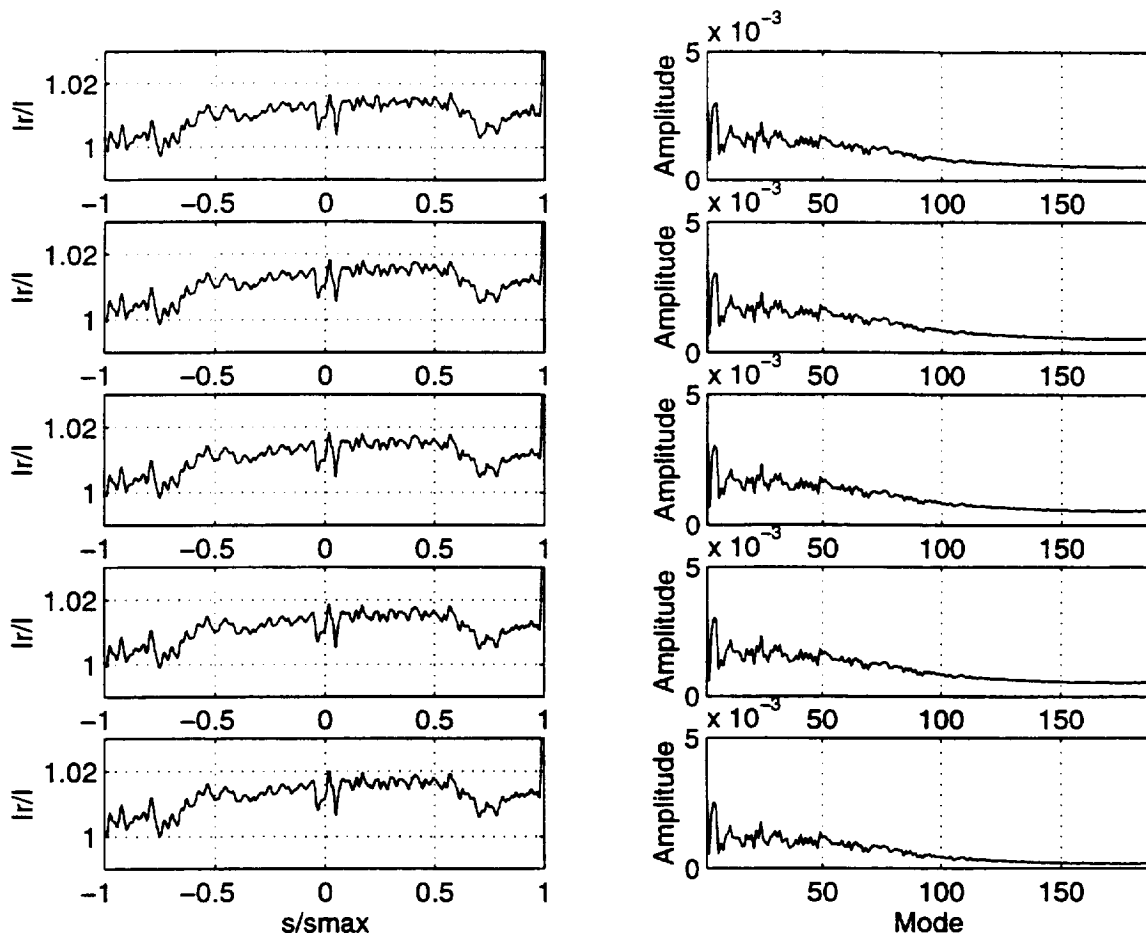
Pressure tap row#3, $\alpha=20$ deg, $\beta=0$ deg, $U=35$ m/s, $C\mu=0$

Top	: 4 images averaged
Second	: 12 images averaged
Third	: 24 images averaged
Fourth	: 36 images averaged
Bottom	: 48 images averaged

Figure 4.2.2 Averaging effects

50

Top left	Luminescence ratio along pressure tap row#3, No smoothing
Top right	Right-hand side calibration plot, No smoothing
Bottom left	Luminescence ratio along pressure tap row#3, After smoothing
Bottom right	Right-hand side calibration plot, After smoothing

Figure 4.2.3 Smoothing effects

Left Hand Side

Right Hand Side

Top   : α=10 deg
Middle : α=20 deg
Bottom : α=30 deg
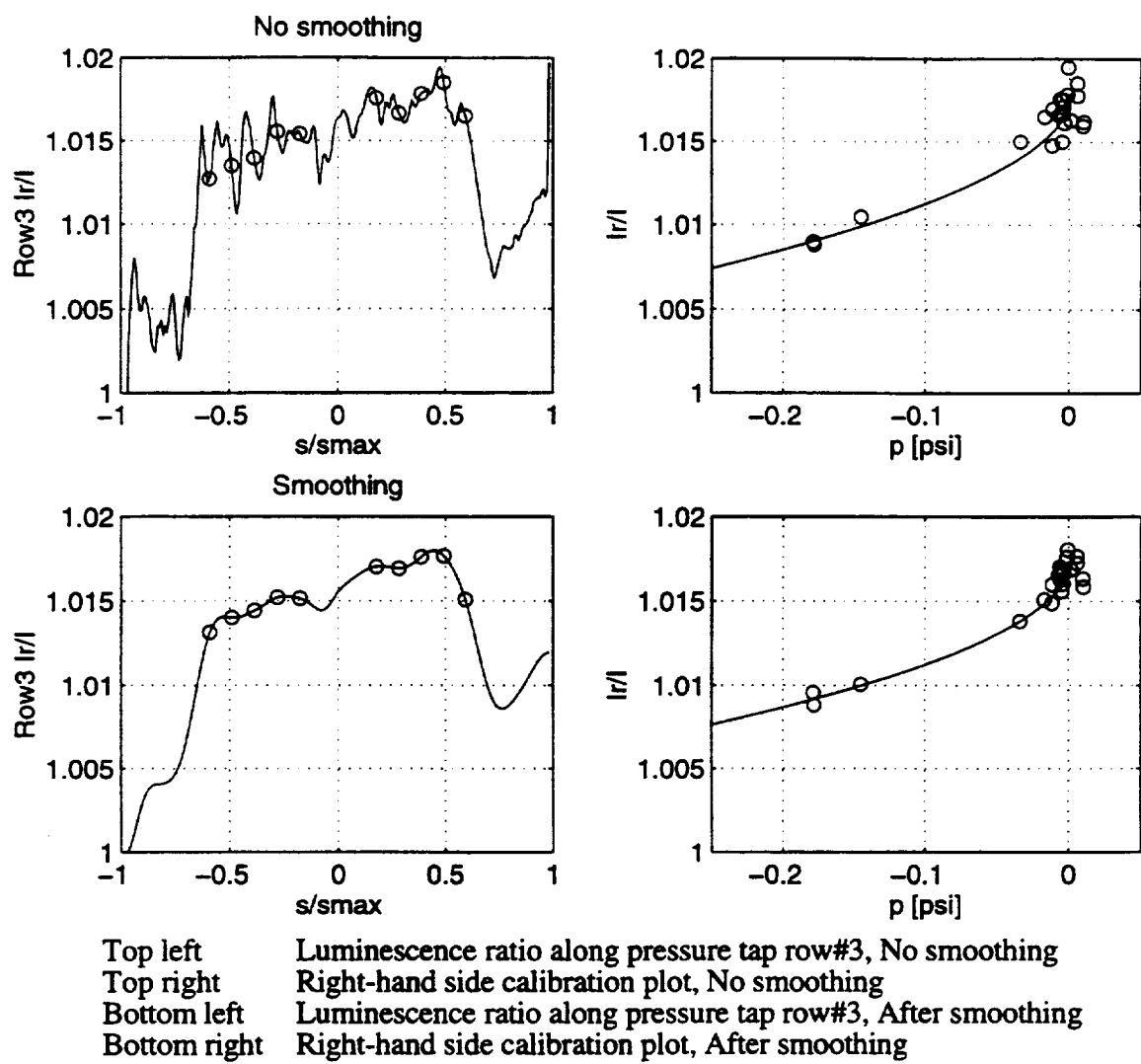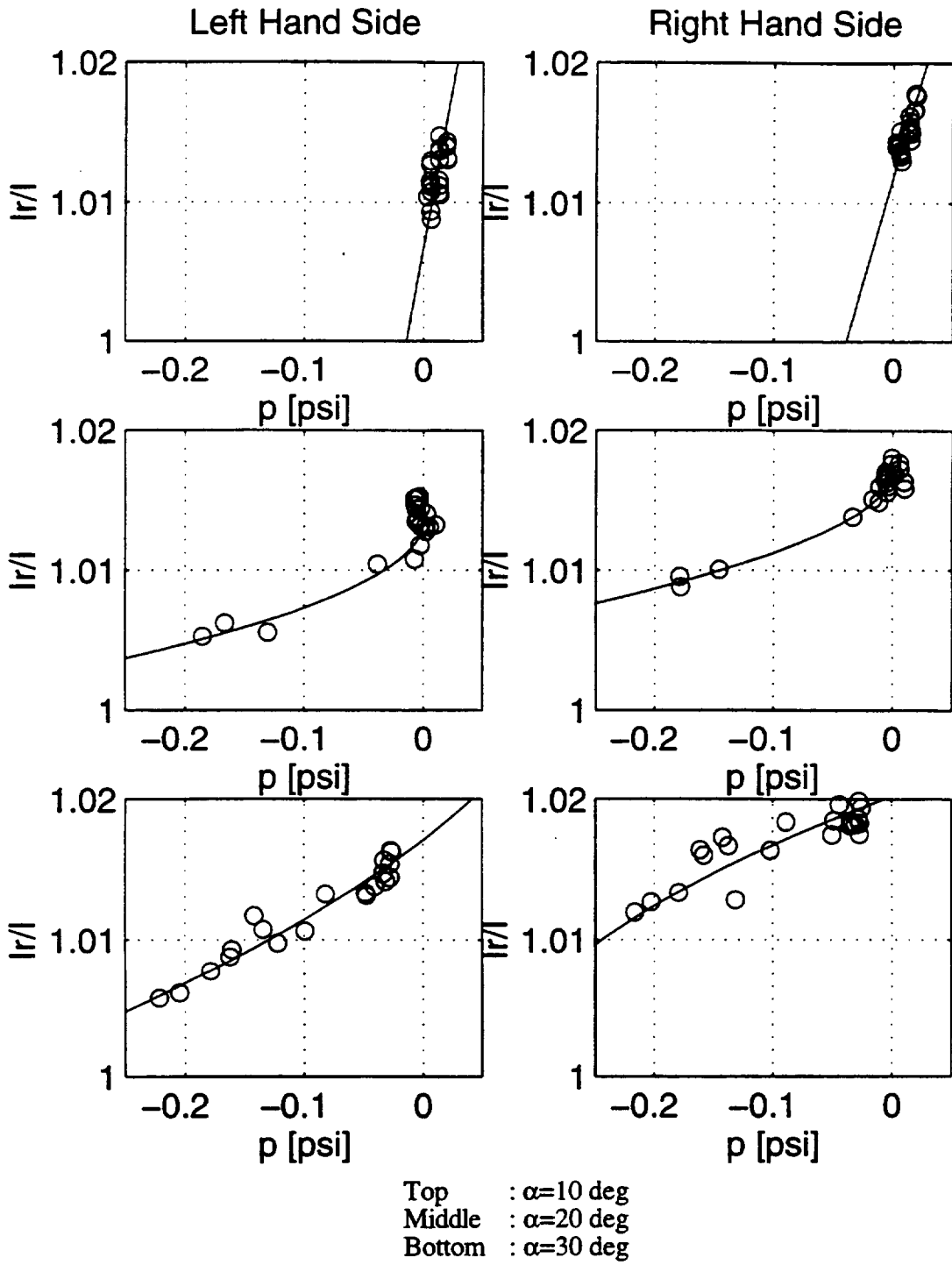
Figure 4.2.4 Typical paint calibration results

Table 4.2.1 Light intensity resolution effects of the 14 bit CCD camera

Location x/C	0.6850	0.6850
Location S/Smax	0.1457	0.7242
Cp	-0.2056	-1.7100
Luminescence @ No-wind	7397.3000	5852.1000
Luminescence @ On-wind	7261.9000	5801.3000
Raw Ir/I	1.0186	1.0088
Ir/I if (No-wind+1)	1.0188	1.0089
Ir/I if (No-wind-1)	1.0185	1.0089
Ir/I if (On-wind+1)	1.0185	1.0086
Ir/I if (On-wind-1)	1.0188	1.0089
Ir/I if (No-wind+1)& (On-wind-1)	1.0189	1.0091
dP (dCp) if (No-wind+1)	-0.0013 psi (-0.010)	0.0045 psi (0.035)
dP (dCp) if (No-wind-1)	0.0006 psi (0.004)	0.0045 psi (0.035)
dP (dCp) if (On-wind+1)	0.0006 psi (0.004)	-0.0092 psi (-0.071)
dP (dCp) if (On-wind-1)	-0.0013 psi (-0.010)	0.0045 psi (0.035)
dP (dCp) if (No-wind+1)& (On-wind-1)	-0.0020 psi (-0.016)	0.0133 psi (0.104)

4.3 Experimental Results

(1) Comparison with pressure tap data

Based on the calibration above, the pressure distribution along the three pressure tap rows at U=35 m/s are compared with the pressure tap measurements in Figure 4.3.1. The pressure sensitive paint data were computed based on the smoothed luminescence ratio data along the row. The circles in the figure indicate the pressure tap data. Generally they agree very well at all angles of attacks and they clearly exhibit the advantage of the pressure sensitive paint as a continuous pressure field measurement. Figure 4.3.2 shows the difference in pressure coefficient Cp between the two measurement methods and most of the points are within ± 0.05 in Cp at $\alpha = 10$ and 20 deg. At $\alpha = 30$ deg, the agreement is not so good as at the lower angles of attack. The calibration tends to deviate from the quadratic approximation and consequently leads to a discontinuity of the pressure around the model center line. This is because the vortical flow over the upper surface becomes unstable at this angle of attack leading to vortex breakdown, as is further discussed later. The pressure tap data measured by the

scanivalve in a rather short time period (several seconds) might be different from the average pressure sensed by the pressure sensitive paint while 48 on-wind images were captured (typically a total time period of 3 minutes).

(2) Angle of attack effects

The angle of attack effects at no sideslip and no blowing conditions are shown in Figure 4.3.3 as whole pressure field images. Each of these pressure distribution images was created from the final luminescence ratio image and any further smoothing or filtering was not applied beyond step 7 of the data reduction sequence. At α=10 deg, the pressure on the whole upper surface is almost uniform because the leading edge vortices are rather weak at this angle of attack. Increasing the angle of attack to 20 deg, clear suction regions appear on the both sides of the model. These are generated by the leading edge separation vortices and the inner straight line dividing the near-zero pressure region and the suction region on each side corresponds to the primary separation line. By further increasing the angle of attack up to 30 deg, the suction pressures near the apex become higher, but they disappear at around the mid chord point. This is because the leading edge separation vortices become stronger as the angle of attack is increased, but then vortex breakdown occurs around the mid chord and the suction is lost. Figure 4.3.4 shows the smoothed pressure distribution at each angle of attack along eight rows indicated in Figure 4.3.5. This figure also shows the formation of the leading edge separation vortex at higher angles of attack. The vortex breakdown can also be detected at α=30 deg from the stronger suction than α=20 deg at front four rows and weaker suction at rear three rows. But clearly pressure sensitive paint is a useful tool to visualize the whole pressure field and it provides much more quantitative information about the flow field than conventional oil flow visualization.

(3) Sideslip effects

The effects of five degrees sideslip angle at 35 m/s with no blowing are shown in Figure 4.3.6 as a pressure field. There is no big change at α=10 deg, but a broader and higher suction region on the windward side than the leeward side at α=20 deg indicates that the vortex on the windward side is stronger and closer to the surface. At α=30 deg, the vortex breakdown location moves forward on the windward side and backward on the leeward side compared to the no sideslip case. This is a consequence of the stronger leading edge separation vortex on the windward side.

54

(4) Free-stream velocity effects

The pressure distribution at three angles of attack are compared at free-stream velocities of 35m/s and 25m/s in Figure 4.3.7. Clearly the 25m/s images show an inferior quality because the pressure changes between the no-wind and on-wind conditions are small and consequently the signal-to-noise ratios are also small, even after a series of corrections. Figure 4.3.8 shows the calibration results at two free-stream velocities at α=20 deg. The minimum pressure difference for a quantitative pressure sensitive paint measurement was found to be about 0.2 psi in this particular experiment.

(5) Model effects

For the model without pressure taps, the paint calibration was carried out using pressure tap data measured by the pressure model for the same test conditions. The pressure field images are compared in Figure 4.3.9 and there is a slight difference between the results from the two models. This indicates that the quantitative pressure measurement using an in-situ calibration is possible for the model without pressure taps if the pressure data are available from other sources.

(6) Temperature effects

Although there was a well-behaved, one-to-one mapping between the luminescence ratio and the pressure in the no-blowing cases, there was no such relation in the blowing case. Figure 4.3.10 shows some typical smoothed luminescence ratio results along the three pressure tap rows and the corresponding pressure tap data at α=20 deg with the blowing condition, $C\mu$=0.06 from the right-hand side slot only. Although the pressure tap data show only a small change between the two sides of the wing, the luminescence ratio changes dramatically and consequently the calibration plots show no consistent relation between the luminescence ratio and the pressure. This is because the temperature of the blowing air introduced from the reservoir located outside of the tunnel was lower than that of the free-stream in the wind tunnel. The cooler blowing air from the slot was entrained by the leading edge vortex and scrubbed on the model surface, which produced local regions with reduced temperatures. Therefore the temperature on the pressure sensitive paint layer was no longer uniform and the luminescence of the paint was affected both by the local pressure and the local temperature and even the in-situ calibration could not deal with this temperature effect. This result provides a very

important warning to the users of pressure sensitive paint that temperature control or parallel temperature measurement is necessary if thermal uniformity does not hold on the model. However, even though the quantitative pressure measurement was not possible in this case, the luminescence ratio images with $C\mu=0$, 0.03 and 0.06 in Figure 4.3.11 provide an insight into where the cooler blowing air goes and the figure shows that the leading edge separation vortex indicated by the lower luminescence region is moved outward by the blowing, as was observed by Celik et al. (Ref. 11) in their oil flow visualization studies.

Top	: Pressure tap row#1
Middle	: Pressure tap row#2
Bottom	: Pressure tap row#3
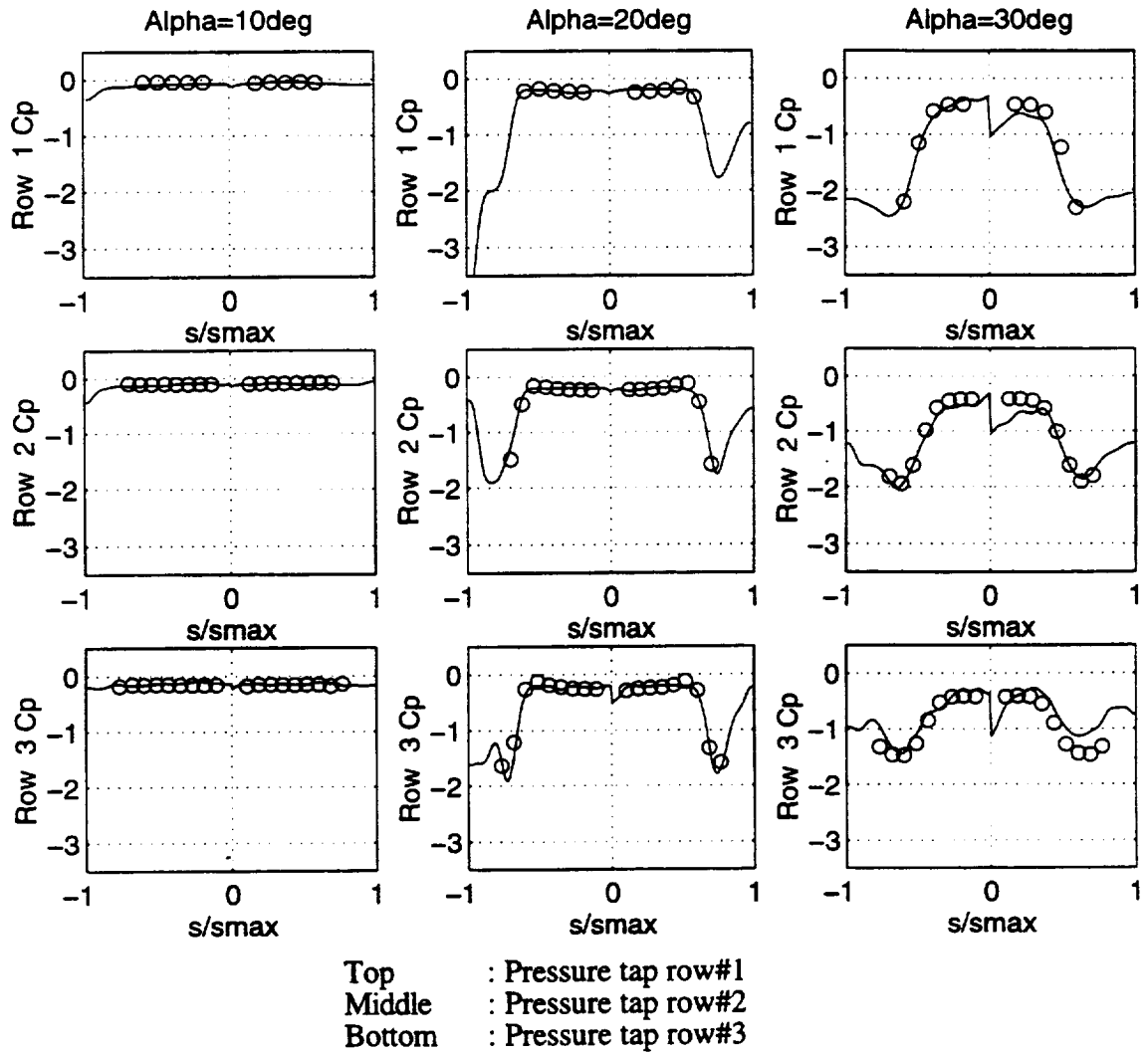
Figure 4.3.1 Comparison between pressure sensitive paint data and pressure tap data
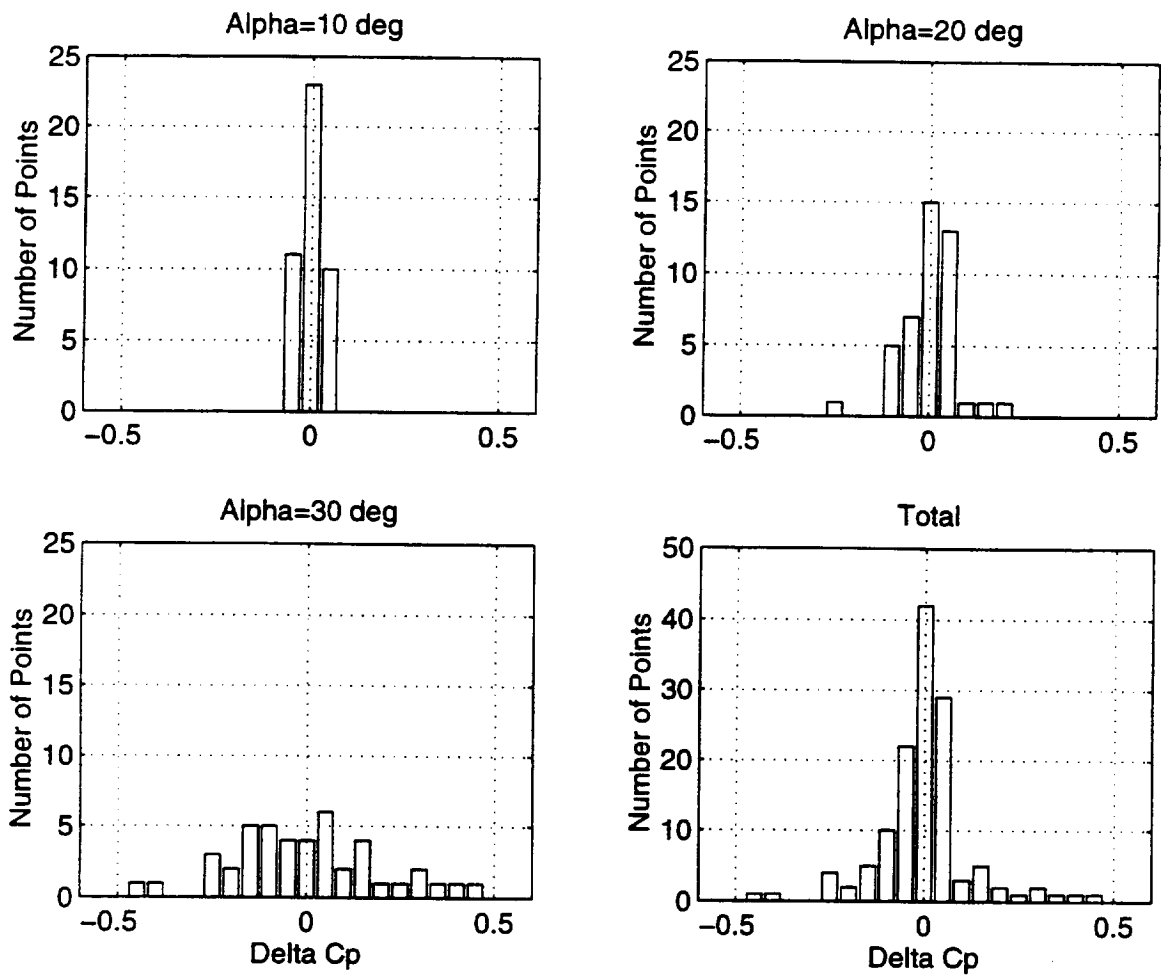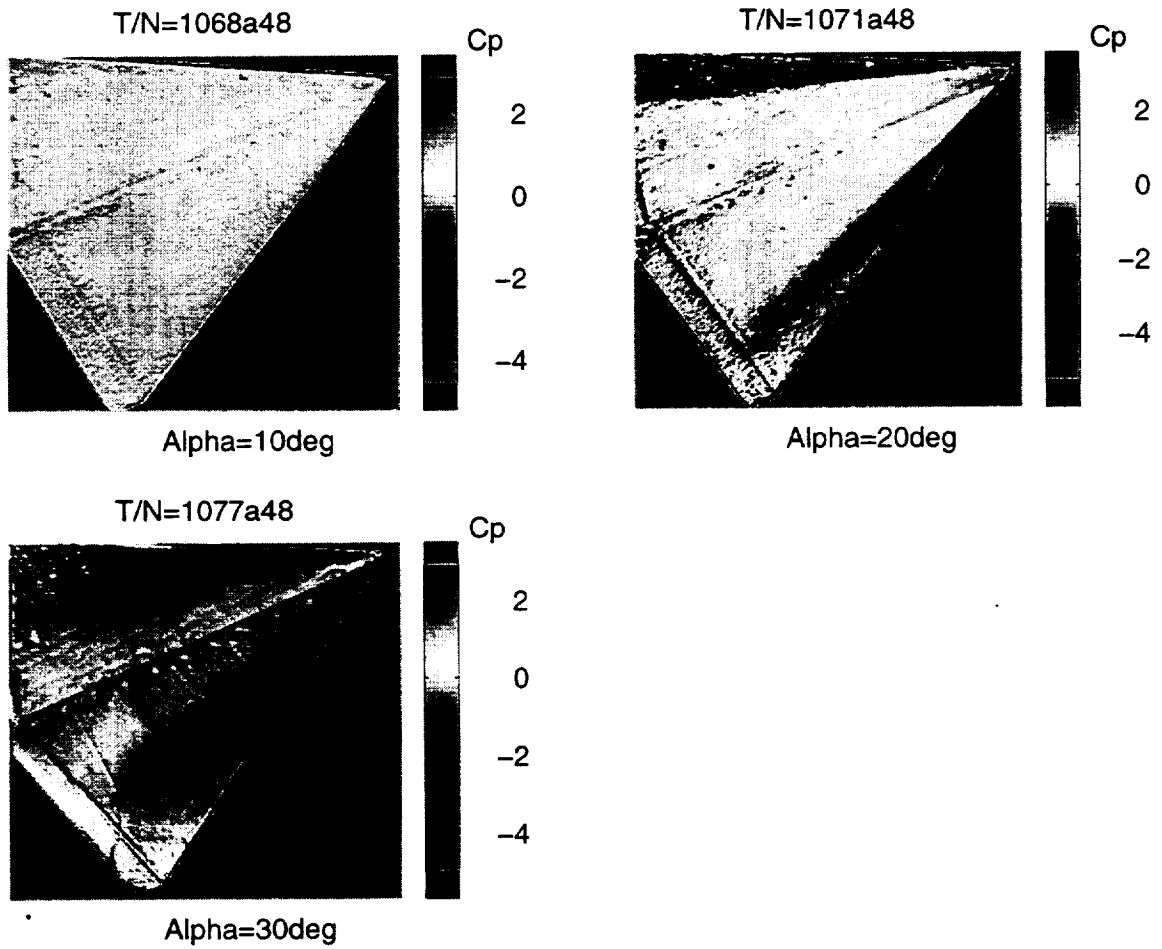
Figure 4.3.2 Overall measurement accuracy

T/N=1068a48

Cp

2

0

−2

−4

Alpha=10deg

T/N=1071a48

Cp

2

0

−2

−4

Alpha=20deg

T/N=1077a48

Cp

2

0

−2

−4

Alpha=30deg

Figure 4.3.3 Angle of attack effects (Whole pressure field)

Beta=0 deg
Cmu=0.00
U=35m/s

Alp=10 deg 1068a48
Alp=20 deg 1071a48
Alp=30 deg 1077a48

── : α=10 deg   ── : α=20 deg   ─ ─ : α=30 deg
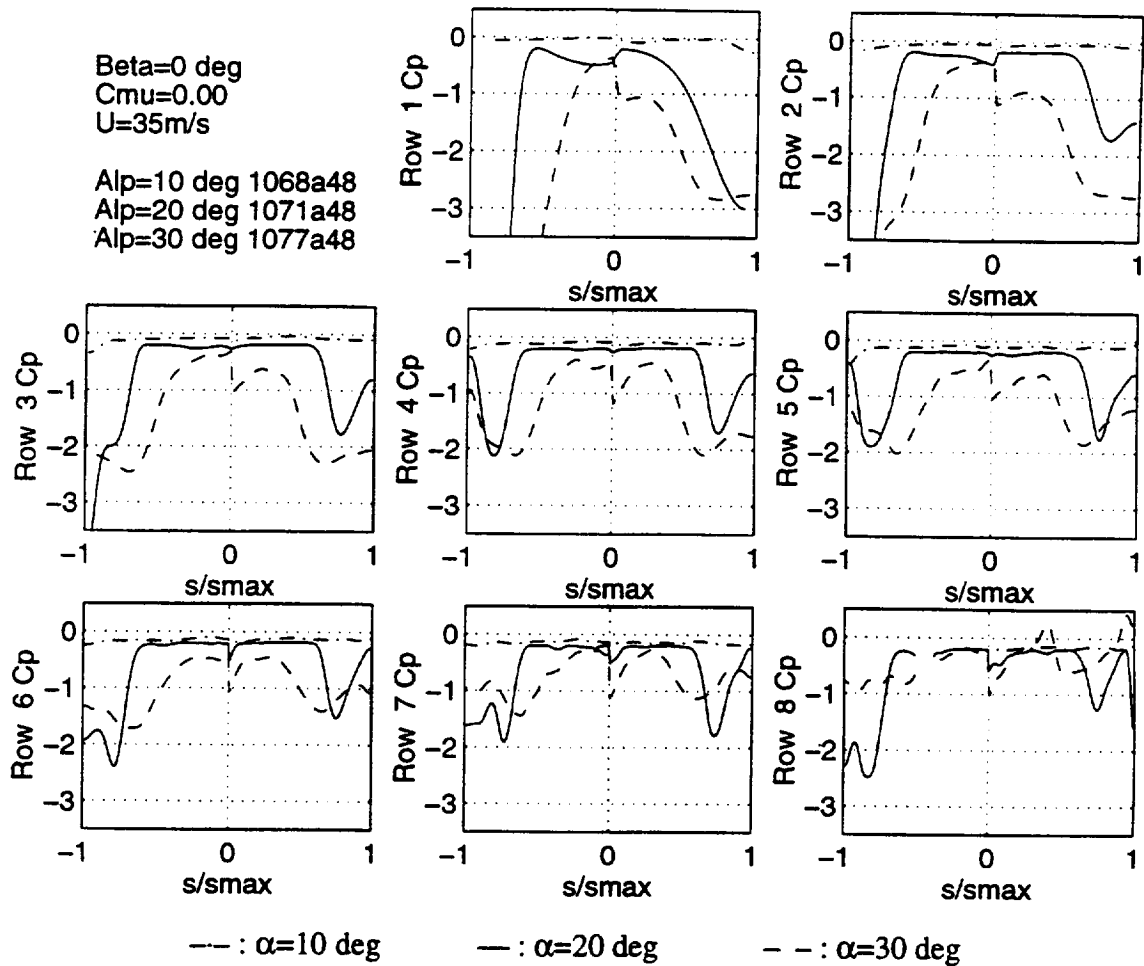
Figure 4.3.4 Angle of attack effects (Pressure distribution along rows)
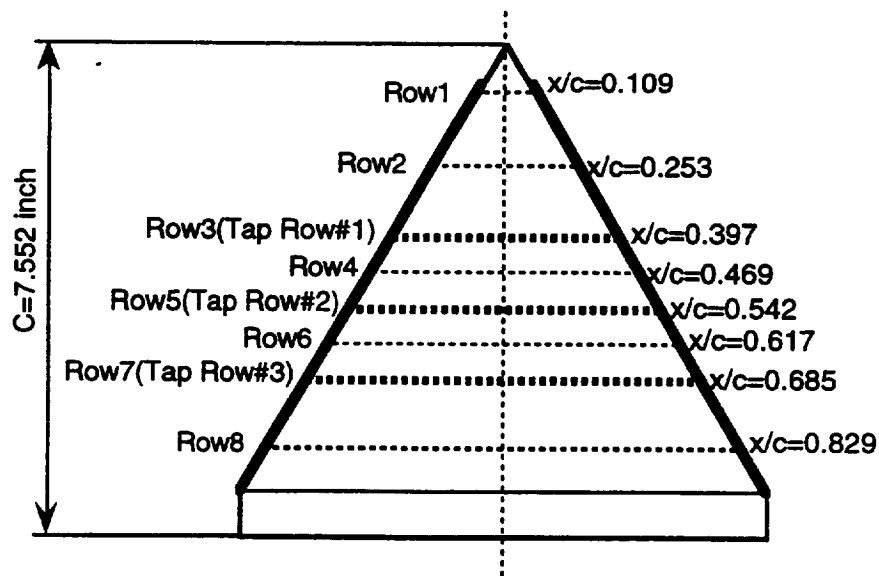
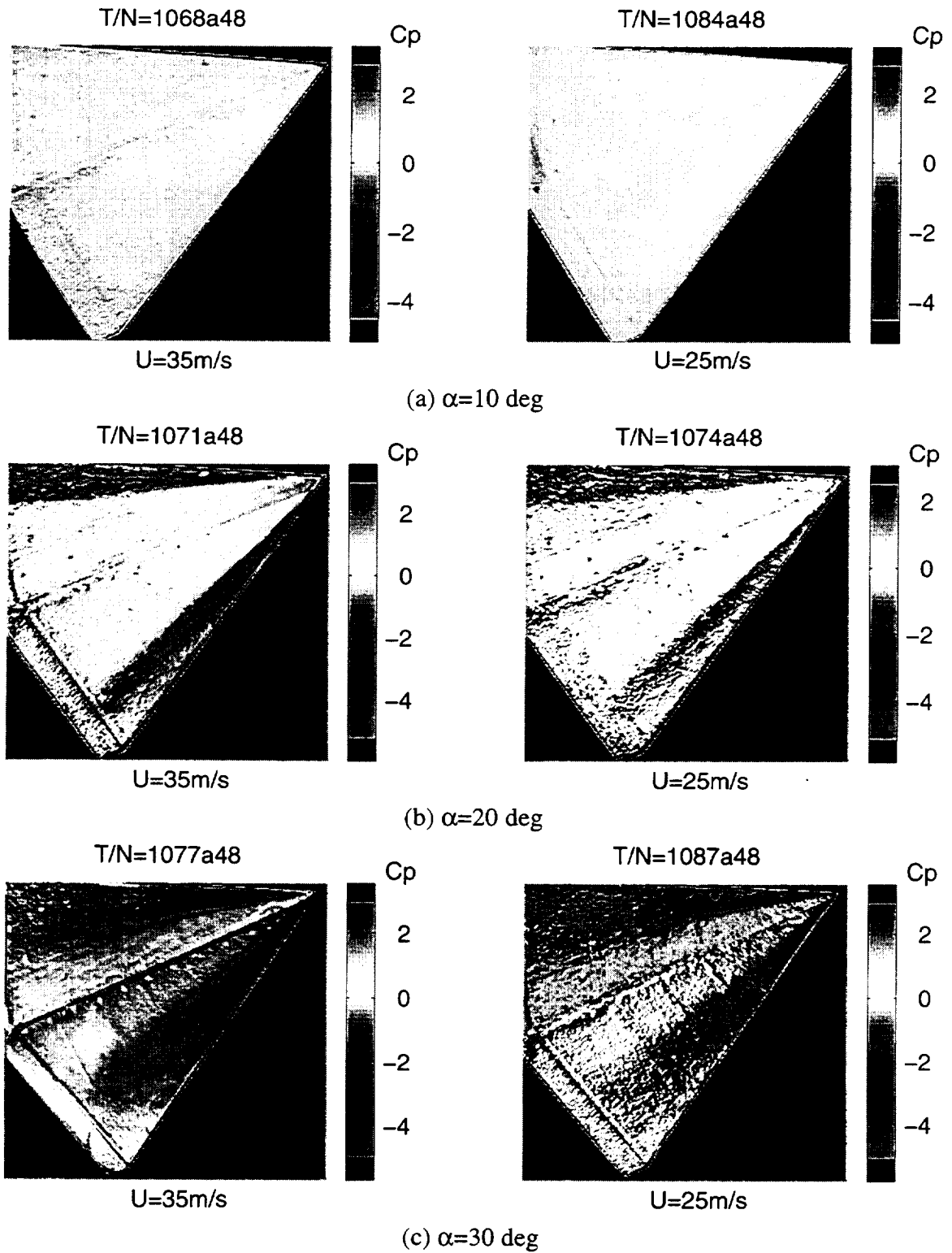Figure 4.3.5 Location of the pressure comparing rows

60

T/N=1068a48

Beta=0deg

T/N=1102a48

Beta=5deg

(a) α=10 deg

T/N=1071a48

Beta=0deg

T/N=1092a48

Beta=5deg

(b) α=20 deg

T/N=1077a48

Beta=0deg

T/N=1097a48

Beta=5deg

(c) α=30 deg
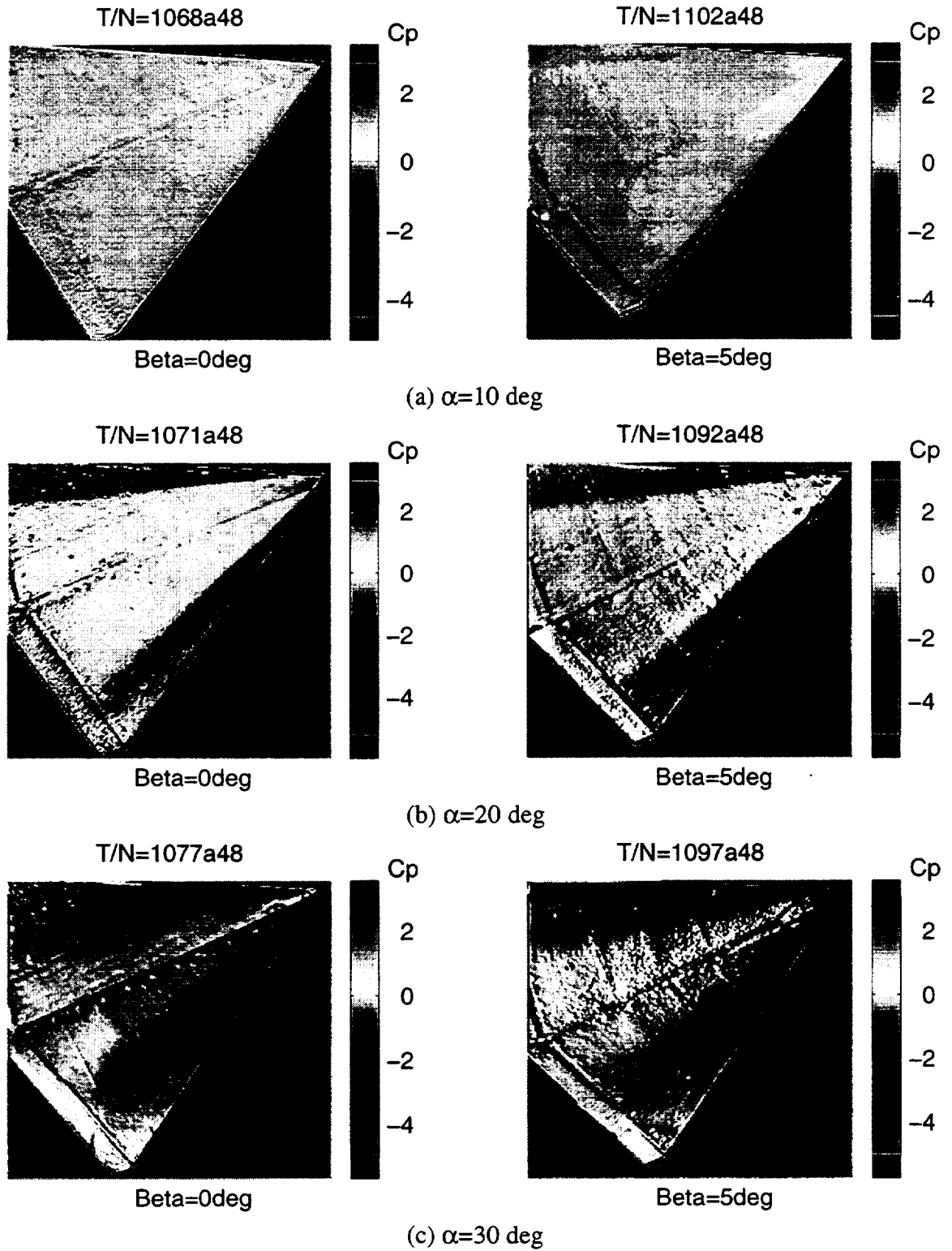
Figure 4.3.6 Sideslip effects

T/N=1068a48

Cp

2

0

-2

-4

U=35m/s

T/N=1084a48

Cp

2

0

-2

-4

U=25m/s

(a) α=10 deg

T/N=1071a48

Cp

2

0

-2

-4

U=35m/s

T/N=1074a48

Cp

2

0

-2

-4

U=25m/s

(b) α=20 deg

T/N=1077a48

Cp

2

0

-2

-4

U=35m/s

T/N=1087a48

Cp

2

0

-2

-4

U=25m/s

(c) α=30 deg

Figure 4.3.7 Free-stream velocity effects
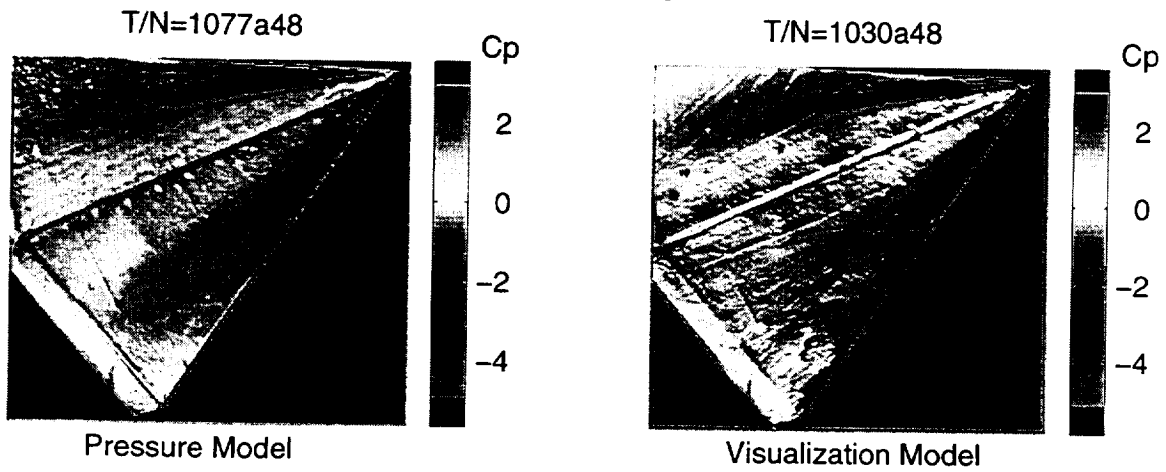
62
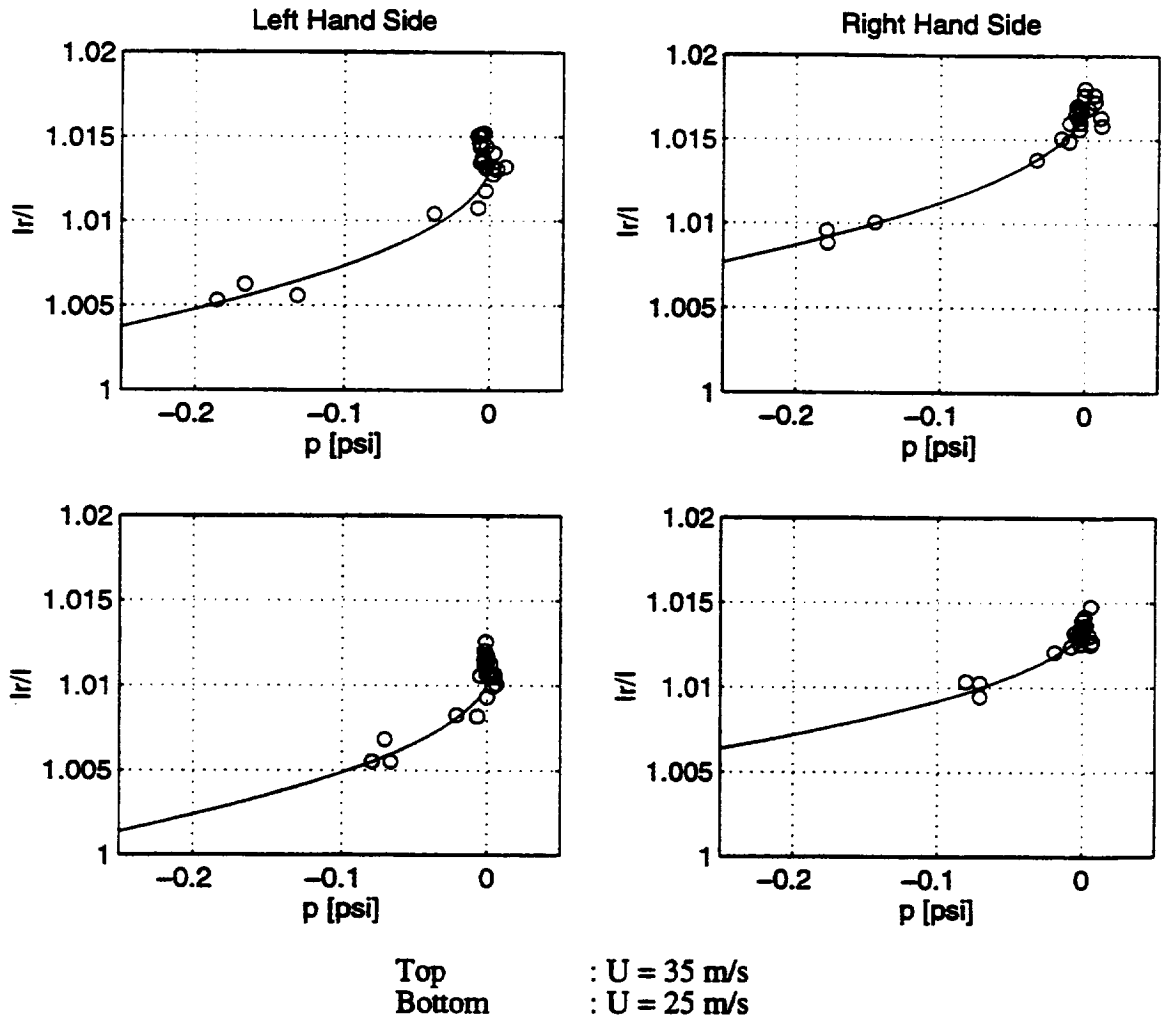
Figure 4.3.8 Free-stream velocity effects for paint calibration

T/N=1068a48

Pressure Model

T/N=1034a48

Visualization Model

(a) α=10 deg

T/N=1071a48

Pressure Model

T/N=1027a16

Visualization Model

(b) α=20 deg

T/N=1077a48

Pressure Model

T/N=1030a48

Visualization Model
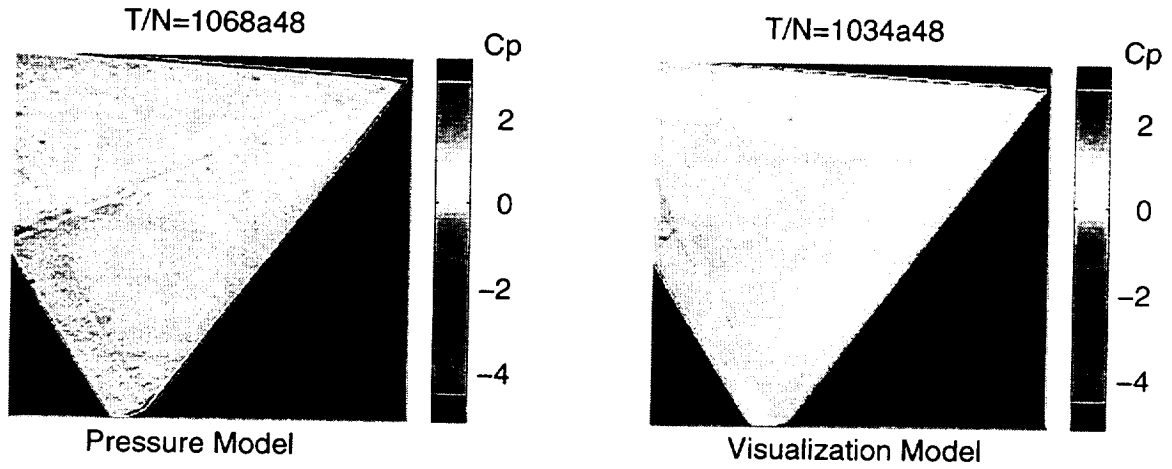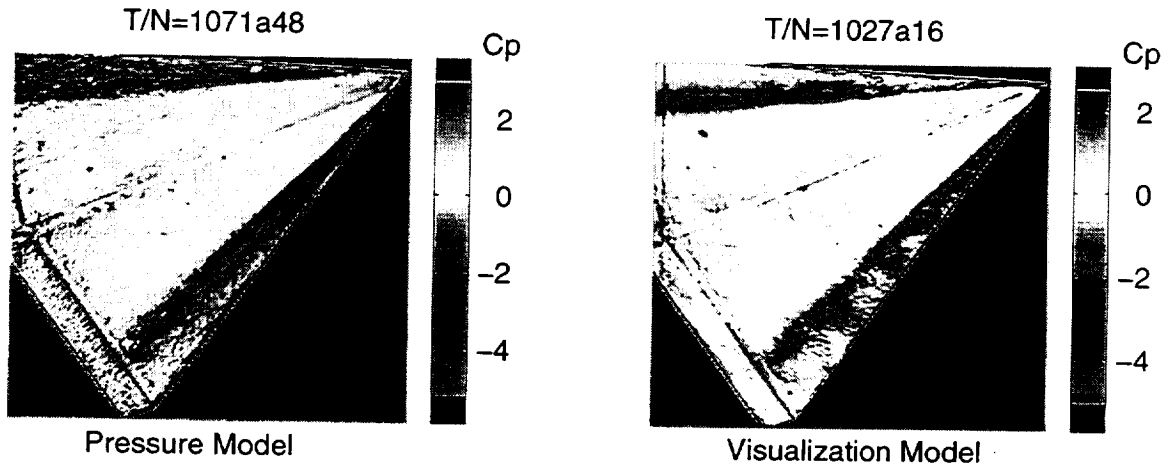
(c) α=30 deg

Figure 4.3.9 Model effects

α=20 deg, β=0 deg, U=35 m/s, Cμ=0.06 (RHS)

Top	Paint calibration
Middle	Luminescence ratio
Bottom	Pressure tap data
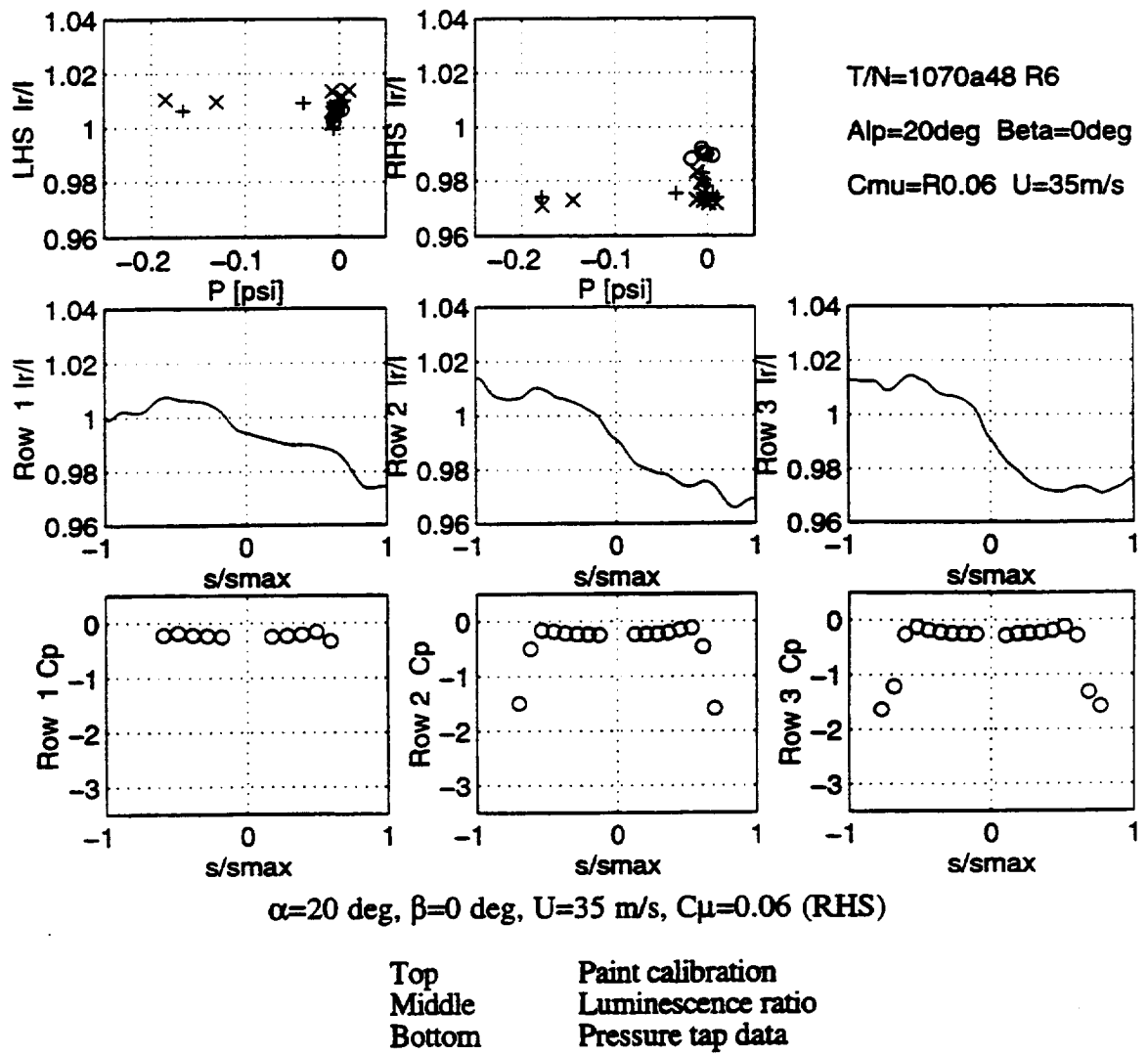
Figure 4.3.10 Typical pressure sensitive paint data with blowing

T/N=1071a48

Cmu= 0.00

T/N=1069a48

Cmu=R0.03
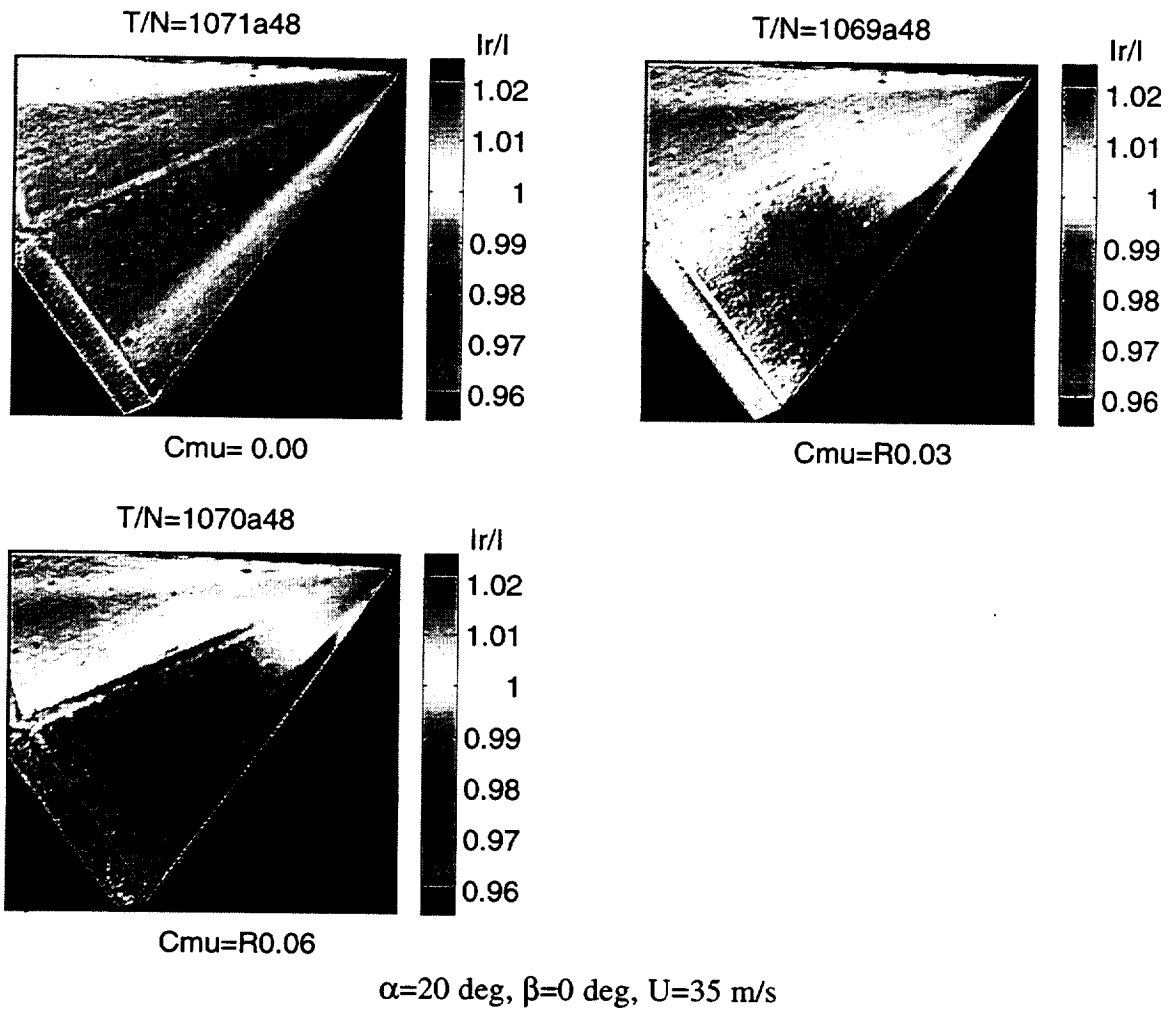
T/N=1070a48

Cmu=R0.06

α=20 deg, β=0 deg, U=35 m/s

Figure 4.3.11 Typical luminescence ratio image with blowing

66

Chapter 5 Unsteady Pressure Measurements

Unsteady pressure measurements were conducted to investigate the applicability of the pressure sensitive paint technique to unsteady flow. The phase lag of the pressure sensitive paint was made up by applying a first-order pole type model.

5.1 Experimental Set-up

The experimental set-up for the unsteady pressure measurements is illustrated in Figure 5.1.1. It was the same set-up as the one used in the impinging jet measurements, including the 8 bit CCD camera and the UV light source. But in the unsteady measurements, the pressure sensitive paint was applied only to a 1" x 1" square region and the unsteady set-up also had a mass flow controller. The mass flow controller supplied a periodically changing mass flow to the jet nozzle and therefore the pressure field on the flat plate also changed periodically. In this mass flow control system illustrated in Figure 5.1.2, the compressed air was divided into two lines and each line was equipped with a valve immediately downstream of the junction. One of the lines was connected to the motor driven rotating ball valve, which generated a periodically changing mass flow rate, and it was merged with another line before they were finally connected to the jet nozzle. This system was capable of controlling both the mean pressure and amplitude of the oscillation by adjusting the

valves after the junction. The time period of the pressure oscillation could also be controlled by the motor speed or the combination of gears connecting the motor axis and the axis of the rotating valve.

An optical interrupter was attached to the axis of the rotating valve and it generated a pulse signal once a every rotation. This pulse was used to start both the image acquisition and the pressure transducer data acquisition exactly at the same phase angle of the periodical pressure change.

As for the pressure transducer data, three small pressure transducers were directly attached to the painted area of the plate, right behind the pressure hole to avoid attenuation and phase delay through the pressure tubing. Pressure data at these three points were sampled at 100 Hz, simultaneously with the paint image acquisition and no filter was applied to the output of the pressure transducers.

The experiment was conducted at only one jet blowing condition with a 12.8 second time period (f=0.078 Hz) and the measurement was repeated five times. The pressure sensitive paint image was recorded on a 80 x 80 pixel array so that the image grabbing board on the computer could store 64 images in its memory without saving them to the hard disk. In each of the five measurements, 16 initial no-wind images were taken first and then 64 on-wind images were taken every 200 ms together with the pressure transducer data. These on-wind images were taken at the same phase angles of the pressure change in each measurement by making use of the trigger signal from the optical interrupter. Finally another 16 images were taken as final no-wind images.

After these five measurements, another set of pressure transducer data were measured with the jet nozzle location shifted 1/8" both in horizontal and vertical direction to increase the pressure tap data points in the same manner as the impinging jet measurements. The effective pressure measuring points are shown in Figure 5.1.3.
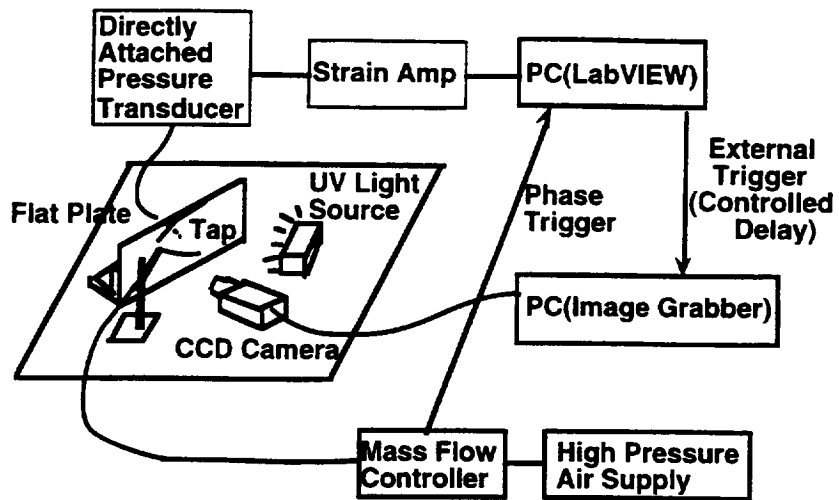
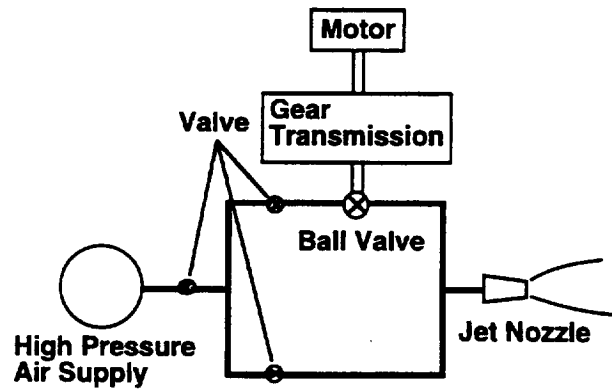Figure 5.1.1 Experimental set-up for unsteady pressure measurements
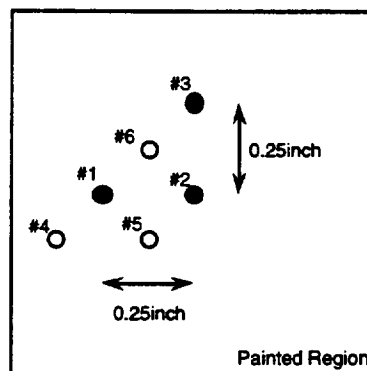

Figure 5.1.2 Mass flow controller

Figure 5.1.3 Pressure measuring points

69

5.2 Data Reduction

(1) Image and Pressure Data Reduction

Each pressure sensitive paint image was reduced in exactly the same sequence as the impinging jet measurements. As there were five images acquired at each of 64 phase angle, the time change of the luminescence ratio was represented by the ensemble average of these five experiments. Pressure transducer data at point #1 to #3, which were measured five times simultaneously with the image acquisition were also represented by the ensemble average of the data at the same phase angle.

(2) Paint response model

The paint response model with the following two assumptions were applied in the data reduction process of the unsteady pressure measurements.

1. There is a simple first-order pole type relation between the time change of the pressure on the paint surface, P(t), and the effective pressure, Peff(t), which determines the luminescence from the paint. Because the pressure sensitive paint works on a diffusion process of the oxygen molecules into the paint layer and on oxygen quenching, it cannot follow the change of the pressure on the surface in infinite time response. Therefore, there should be some phase lag and a first order pole was assumed for simplicity. This relation is expressed in the Laplace transformation form as:

$$\frac{Peff(s)}{P(s)} = \frac{K}{\tau s + 1} \tag{5.2.1}$$

and this relation corresponds to,

$$\tau \frac{dPeff(t)}{dt} + Peff(t) = KP(t) \tag{5.2.2}$$

in the physical time domain.

2. There is a linear relationship between the instantaneous luminescence ratio Ir/I(t) and the effective pressure Peff(t) introduced in the first assumption. This is based on the basic theory of the pressure sensitive paint and the relation is expressed as:

$$\frac{Ir}{I}(t) = A + B\left[\frac{Peff(t)}{Pref}\right] \tag{5.2.3}$$

70

Although the two-line relation worked better, as discussed in the previous chapters, the single linear relation is assumed here in order to make the data reduction simple.

Based on these two assumptions, the time change of the surface pressure can be estimated from the pressure sensitive paint data Ir/I(t) as:

$$Pest(t) = \frac{Pref}{BK}\left[\frac{1}{\tau}\frac{d}{dt}\frac{Ir}{I}(t) + \left\{\frac{Ir}{I}(t) - A\right\}\right]$$

(5.2.4)

(3) Paint calibration

In Eq.(5.2.4), there are three unknowns, (τ, A, BK). To determine these unknowns, pressure measuring point #1, where the pressure change in a period was largest, was chosen as a calibration point. At the calibration point, the time change of the luminescence ratio Ir/I(t) was expressed mathematically by a Fourier series expansion using up to the 10th mode so that the time derivative term could be mathematically computed. The three unknowns were then determined as the combination to minimize the pressure estimation error for 256 points (50 ms interval) in a period given by:

$$Error = \sum_{k=1}^{256} \sqrt{\{Pest(t_k) - P(t_k)\}^2}$$

(5.2.5)

Then, once the combination of the unknowns at the calibration point was found through calibration, they were applied to all other points in the image after the time change of the luminescence ratio was represented by a Fourier series expansion form.

5.3 Experimental Results

(1) Paint Calibration

Figure 5.3.1 shows the luminescence ratio images in one of the five pressure sensitive paint measurements along with the pressure change at the pressure measuring point #1, the calibration point. The calibration result about this point is shown in Figure 5.3.2 and the values for the three unknowns were found to be:

$$\tau = 0.4223 \text{ [s]}$$

$$A = 1.0233$$
$$BK = 0.15942$$

Assuming B=0.2669, as was computed in Eq.(3.2.8) for the higher pressure region in the impinging jet measurements, the gain of the first-order pole is computed as:
$$K=0.5973$$
Then, the times required for a 90% and 99% recovery to the step change of the pressure are computed from τ and K as:

For 90% recovery $\quad$ K{1-exp(-t/τ)}=0.9 $\quad$ t=-τ log(0.1/K) = 0.75 s

For 99% recovery $\quad$ K{1-exp(-t/τ)}=0.99 $\quad$ t=-τ log(0.01/K) = 1.73 s

These are faster than the 90% response time of this PtOEP/GP-197 combination (2.5 second) measured in a special chamber at the University of Washington (Ref. 12).

The overall gain of the first-order pole starts falling down from the cut-off frequency and it is given by:

$$2\pi f\tau=1 \Rightarrow f=1/(2\pi\tau)=0.377 \text{ Hz}$$

Therefore, from the sampling theory, f=0.188 Hz, which is equivalent to a time period of 5.3s, is the limit frequency for this particular PtOEP/GP-197 type pressure sensitive paint. But, once more faster paint is available, the same approach described above can be applied to enhance the unsteady pressure measurement capability.

(2) Estimated pressure

The estimated pressure and the surface mounted pressure transducer data are also compared in Figure 5.3.3. At the pressure measuring point #6, which is close to the calibration point, the estimated unsteady pressure, Pest(t), agrees well both in the pressure rising portion and the pressure dropping portion. However, it shows some disagreement in the constant pressure regions. One of the reasons for this is that the first term of Eq. (5.2.4) is dominant and only a slight discontinuity in the slope generates a huge change in the estimated pressure. This problem might be solved by increasing the number of experiments over which to ensemble average and by improving the light intensity resolution of the CCD camera. At the other points, pressure measuring point #2 which is 1/4" away from the calibration point, the result shows a poor agreement. The tendencies of pressure rise and pressure drop are captured, but the pressure level does not

agree here. This is probably because the local pressure decreases to a level where the assumption of a single linear relation between the luminescence ratio (Ir/I) and pressure ratio (P/Pref) does not hold anymore. As the current model assumes a linear relation, with a smaller inclination in the higher pressure region, a smaller luminescence ratio leads to a much lower pressure than is the case. Trying to deal with the two-line calibration, the whole system become non-linear and very hard to solve.

(3) Future model refinement

To deal with unsteady pressure measurements more accurately, we should get deeper into the physics of the pressure sensitive paint: oxygen diffusion and oxygen quenching.

As is described in Ref. 13, the diffusion process of the oxygen molecules is subject to the one dimensional unsteady diffusion equation:

$$\frac{\partial^2 [O_2]}{\partial X^2} = \frac{1}{Dm}\frac{\partial [O_2]}{\partial t} \tag{5.3.6}$$

under the boundary conditions:

$$[O_2](d,t) = P_{O2}(t)/kT$$

$$\left.\frac{\partial [O_2]}{\partial t}\right|_{X=0} = 0 \tag{5.3.7}$$

where X=0 is the paint surface and X=d is the bottom of the paint layer.

Then the time and position dependent oxygen concentration in the paint layer has to be related to the luminescence from the paint, but the chemical reaction is no longer in equilibrium and the contribution from each location within the layer to the paint luminescence should be taken into account.
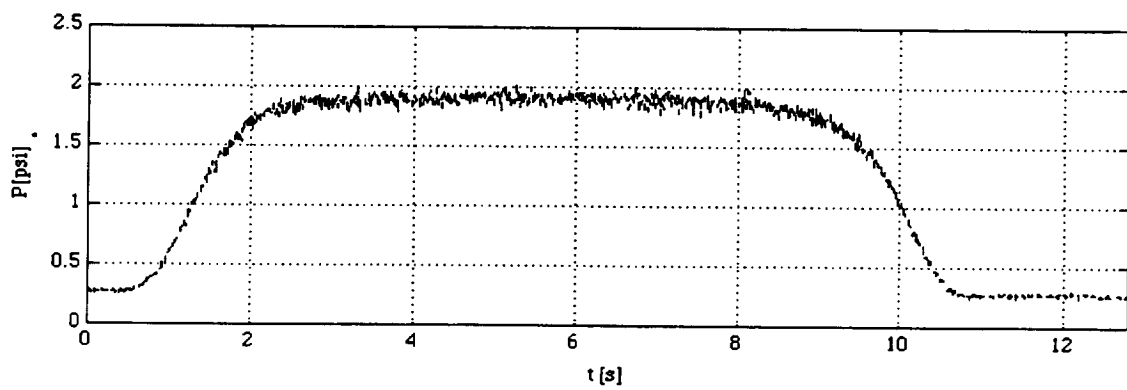
(4) Faster pressure sensitive paint

In contrast, extensive work has been conducted to develop a faster pressure sensitive paint, which no longer needs the modeling described above. As long as the luminescent substance is distributed in an oxygen permeable polymer binder, the response time is limited because the diffusion process of the oxygen exists there. This problem can be solved by putting the luminophor directly onto the surface and Ref. 12 reported a faster paint with a response as fast as a few milliseconds. Some techniques and paints are also

73

introduced in Ref. 12 and one of the ways under development at the University of Washington is to make the luminophor absorb into fine silica particles and attaching them onto the surface by glue. But the surface roughness tend to become coarse and the robustness of the paint becomes poor in this kind of painting method. And the biggest problem is that these faster paints are not commercially available at present.
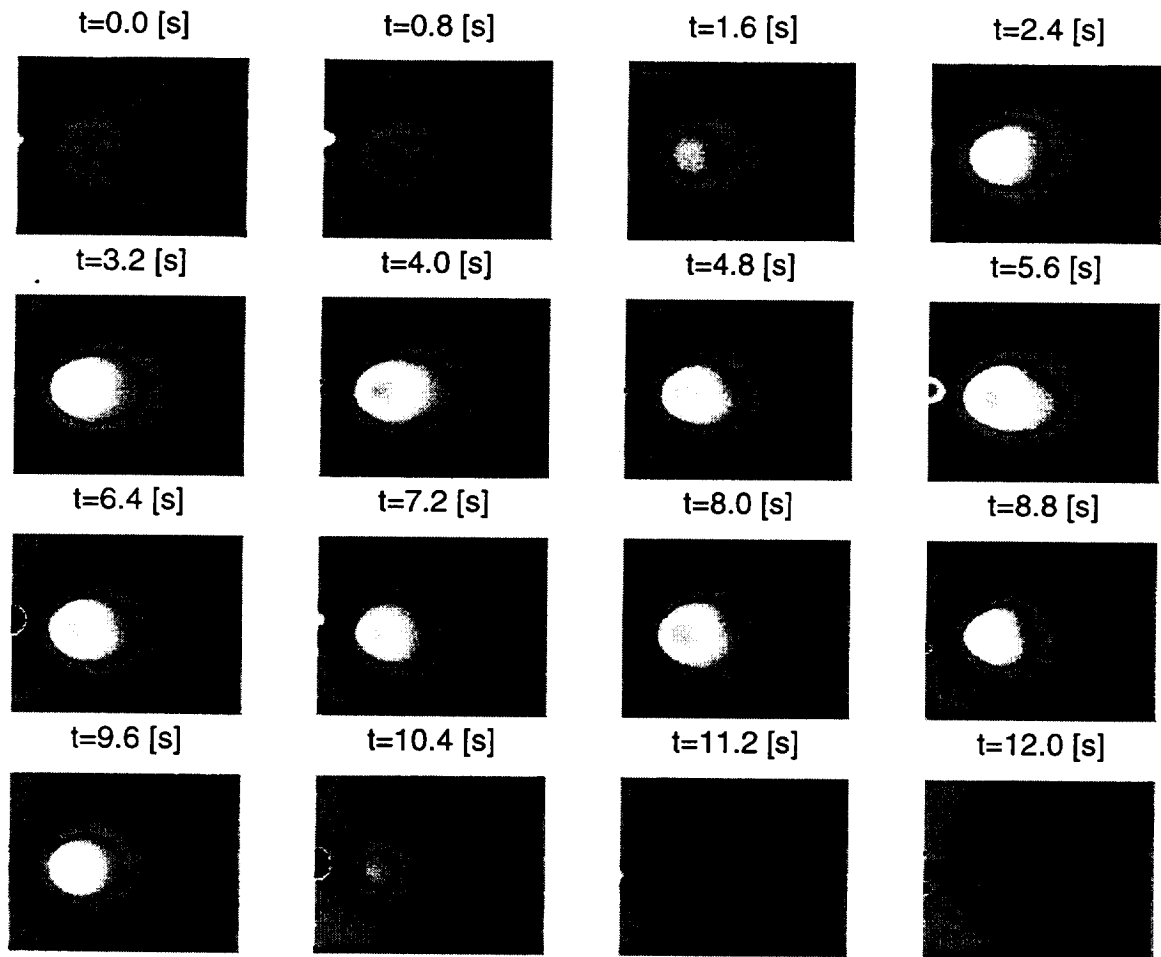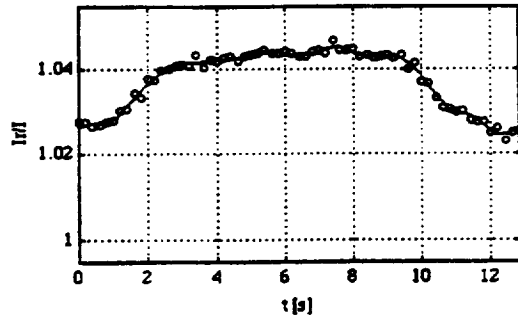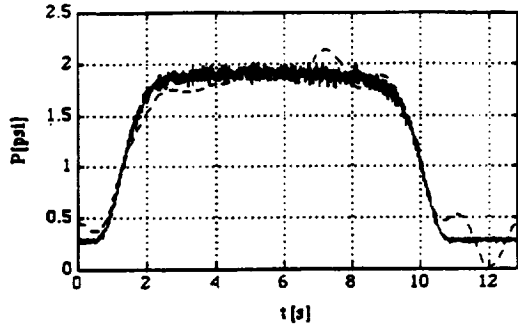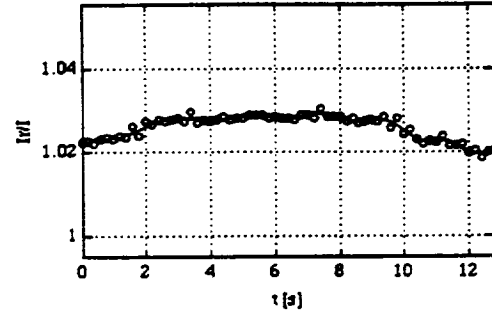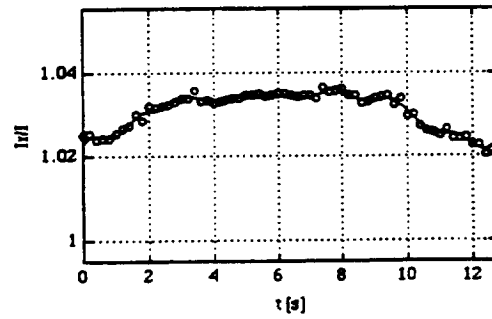
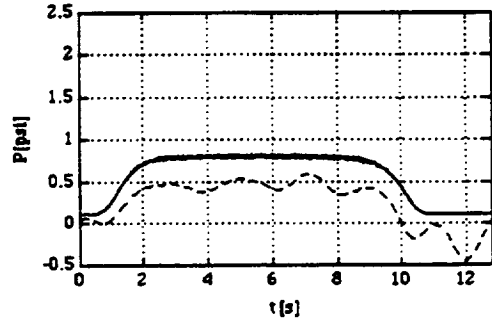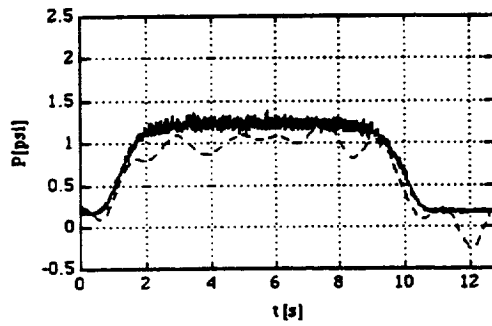(a) Luminescence ratio images

(b) Pressure change at calibration point

Figure 5.3.1 Time change of the luminescence ratio field

— : Pressure transducer data
- - : Pressure sensitive paint data

Figure 5.3.2 Unsteady paint calibration result

— : Pressure transducer data
- - : Pressure sensitive paint data

Figure 5.3.3 Estimated unsteady pressures (Left : Point #6, Right Point #2)

76

Chapter 6   Conclusions

6.1 Conclusions

(1) A pressure sensitive paint technique using a commercially available PtOEP/GP-197 was established and applied to the impinging jet measurements.

(2) An in-situ calibration using five pressure tap data points dealt with the two-line calibration and achieved about a 0.1 psi pressure resolution in the impinging jet measurements.

(3) The pressure sensitive paint technique was expanded to low-speed wind tunnel tests by using a high grade CCD camera and applying a series of corrections to improve the measurement accuracy.

(4) Pressure sensitive paint applied to a delta wing showed a great capability of the technique both as a pressure measurement tool and as a pressure field visualization tool even at velocities as low as 35 m/s.

(5) Temperature control or a parallel temperature measurements is necessary if thermal uniformity does not hold on the model.

(6) A simple first-order pole model showed a possibility to expand the pressure sensitive paint technique to unsteady pressure measurements. To improve the measurement accuracy, further refinement of the model which includes the physics of the oxygen diffusion and the oxygen quenching are required.

(7) Response time of the PtOEP/GP-197 was found to be 0.75s for a 90 % recovery and 1.73s for a 99% recovery to the step pressure change. The maximum frequency resolved by this pressure sensitive paint was found to be 0.188 Hz.

6.2 Future Work

From the pressure sensitive paint user's point of view, the following ideas are suggested for possible future work.

(1) More aeronautical and engineering application : The more complicated the flow field is, the more powerfully the pressure sensitive paint technique can work. A forebody/wing vortex interaction with tails, a load analysis of the stores and/or bombs installed on the lower surface are possible practical applications for the fighter type airplane. Flow fields including separation, such as a high lift configurations of the airplane and flow field analysis of cars are possible examples of low-speed applications.

(2) PMT measurement : PMT (Photomultiplier tube) is another option to measure the luminescence from the pressure sensitive paint. This is a point measurement of the luminescence and can be applied to the surface where optical access for the CCD camera is not necessarily good. It is also useful for measuring the pressure of rotating machinery, such as a helicopter rotor or turbine blade.

(3) Further modeling for unsteady pressure measurement : Further modeling based on the physics of the pressure sensitive paint is required for more accurate unsteady pressure measurement.

(4) Collaboration with physicists and chemists: People in the aerodynamics field need not necessarily get deeply into the development of the paint itself. This work should be assigned to the physicists and chemists, but close collaboration with them is essential for improving the pressure sensitive paint technique.

References

(1) Vollan A. and Alati L., A New Optical Pressure Measurement System (OPMS), 14th ICIASF Congress, OCT. 1991, Rockville, MD.

(2) McLachlan B. G., Bell J. H., Kennely R. A., Schreiner J. A., Smith S. C., Strong J. M., Gallery J. and Gouterman M., Pressure Sensitive Paint use in the Supersonic High-Sweep oblique Wing (SHOW) Test, AIAA-92-2686

(3) Bell J. H. and McLachlan B. G., Image Registration for Luminescent Paint Applications, AIAA-93-0178

(4) McLachlan B. G., Kanvandi J. L., Callis J. B., Gouterman M., Green E., Khalil G. and Burns D., Surface pressure field mapping using luminescent coatings, Experiments in Fluids 14 (1993) pp. 33-41

(5) Morris M. J., Donovan J. F., Kegelman J. T., Schwab S. D., Levy R. L. and Crites R. C., Aerodynamic Application of Pressure-Sensitive Paint, AIAA-92-0264

(6) Crites R. C., Measurement Techniques — PRESSURE SENSITIVE PAINT TECHNIQUE, von Karman Institute for Fluid Dynamics, Lecture Series 1993-05

(7) Morris M. J., Benne M. E., Crites R. C. and Donovan J. F., Aerodynamic Measurements Based on Photoluminescence, AIAA 93-0175

(8) Donovan J. F., Morris M. J., Pal A., Benne M. E. and Crites R. C., Data Analysis Techniques for Pressure- and Temperature-Sensitive paint, AIAA-93-0176

80

(9) Liu T., Campbell B. T., Burns S. P. and Sullivan J. P., Temperature and Pressure-Sensitive Luminescent Paints in Aerodynamics, to be published

(10) Fox M. D., Kurosaka M., Hedges L. and Hirano K., The influence of vortical structures on the thermal fields of jets, J. Fluid Mech. (1993), vol. 255, pp. 447-472

(11) Celik Z.Z. and Roberts L., Vortical Flow Control on a Delta Wing by Lateral Blowing, AIAA 94-0509

(12) Baron A. E., Denielson J. D. S., Gouterman M., Wan J. R., Callis J. B. and McLachlan B., Submillisecond response times of oxygen-quenched luminescent coatings, Rev. Sci. Instrum. 64(12), Dec. 1993 pp. 3394-3402

(13) Carroll B., Abbitt J., Lukas E. and Morris M., Pressure Sensitive Paint Response to a Step Pressure Change, AIAA 95-0483